Kaya-guided hybrid deep learning for leave-country-out estimation of national CO_2 emissions: a 112-country benchmark with country-clustered inference, conformal uncertainty, and explainable AI

Samiuel C. Atuahene[1,2], Bismark Boateng[1], Hilda Amarfio[3], Ekow Yaleh Quayson[1]

Francis Boateng Agyenim[1],

[1]Emerging Engineering Technologies Division, CSIR, Institute of Industrial Research, East Legon, Accra, Ghana

[2]Research and Development Department, Premium Intelligence Networks and Systems Co. Ltd., Accra, Ghana

[3]Department of Maternal and Child Health Nursing, School of Nursing & Midwifery, College of Health Sciences, University of Ghana, Legon, Accra.

[*] Corresponding author: Samiuel C. Atuahene

Abstract

Reliable national CO_2 inventories underpin the Paris Agreement's Enhanced Transparency Framework, yet many non-Annex I countries lack complete emission statistics. We reframe national emissions modelling as *leave-country-out* (LOCO) estimation: predicting a country's per-capita CO_2 from eight-year trajectories of energy and socioeconomic covariates, with no access to its own emission history. Using Global Carbon Budget and Energy Institute data harmonized by Our World in Data, we build a 112-country panel (1990-2023; 3,024 windowed samples) and benchmark thirteen models under country-disjoint five-fold cross-validation. The proposed Kaya-guided CNN-BiLSTM-Attention network (KG-CBA) couples a log-linear backbone motivated by the Kaya identity to a convolutional-recurrent-attention branch that learns only the nonlinear residual, tuned by particle swarm optimization. Because the sample contains 27 repeated years per country, all inference is country-clustered. Kaya guidance significantly improves the unguided architecture (median APE 15.7% vs 20.8%, $p = 0.002$), and ridge regression significantly outperforms every tree ensemble and every unguided deep network; but the best ensemble's apparent edge over ridge is not significant (15.1% vs 16.3%, $p = 0.22$), where observation-level testing would report $p < 10^{-9}$. Error is highly concentrated: six structurally atypical energy systems contribute 79-84% of total squared error. Adding the low-carbon energy share on a 76-country sub-panel halves median error (7.35% vs 13.72% like-for-like), showing that energy-mix data availability, not model sophistication, is the binding constraint. Removing all CO_2-derived covariates costs under one percentage point, so the estimator suits countries with no inventory at all. Split-conformal Monte-Carlo-dropout intervals reach 81.9% coverage at a 90% nominal level, the shortfall traced to non-exchangeability under grouped splits. In conventional temporal forecasting, learners beat naive persistence only marginally and inconsistently across evaluation windows. Data and code are open.

Keywords: CO_2 emissions; hybrid deep learning; Kaya identity; clustered inference; conformal prediction; explainable artificial intelligence; greenhouse gas inventories; Africa

1. Introduction

Anthropogenic carbon dioxide remains the dominant driver of observed warming, and fossil CO_2 emissions reached record levels again in 2024 [1,2]. Article 13 of the Paris Agreement obliges all parties to report national greenhouse-gas inventories under the Enhanced Transparency Framework, yet the reporting landscape is deeply uneven. Only a minority of non-Annex I countries submit complete and timely inventories, and independent assessments find the largest inter-source discrepancies precisely where capacity is lowest, notably across sub-Saharan Africa [3-5]. Gap-filling therefore matters: mitigation planning, carbon-market integrity, and the global stocktake all depend on emission estimates for countries whose own statistical systems cannot yet produce them [5,6].

Machine learning has been proposed as a pragmatic response. Recent work spans subnational gap-filling for G20 jurisdictions [6], sectoral emission prediction for African economies [7-10], and a rapidly growing literature on deep and hybrid architectures for CO_2 forecasting [11-18]. Within that literature, hybrid designs that stack convolutional feature extractors, recurrent sequence models, and attention mechanisms, often tuned by metaheuristic algorithms, now dominate methodological claims of state-of-the-art accuracy [13-15,19-21].

Four weaknesses limit the practical value of much of this evidence base. First, most studies evaluate *temporal* forecasting for countries whose emission history is fully observed, precisely the setting where inventories already exist, rather than the *cross-country generalization* setting that the inventory-gap problem poses. Second, validation protocols frequently allow the same country to appear in both training and test data, inflating reported skill through country-specific memorization. Third, naive benchmarks are routinely absent; national per-capita emissions are highly persistent from year to year, and without a persistence baseline, near-unity coefficients of determination are easily mistaken for skill [22-24]. Fourth, and least remarked, significance is almost always assessed by treating every country-year as an independent observation. Panel emission data are strongly clustered within countries; observation-level tests on such data understate standard errors by roughly the square root of the cluster size, and can render a fraction of a percentage point "highly significant".

This paper addresses all four. We formalize national emissions estimation as a leave-country-out (LOCO) problem: given only eight-year trajectories of six widely available covariates, predict a country's per-capita CO_2 without access to its own emission record. Because the target country contributes no training information, persistence is undefined and the task isolates genuine covariate-to-emissions generalization. All inference is clustered at the country level. All experiments use measured data anchored in the Global Carbon Budget [2] and the Energy Institute Statistical Review [25], as harmonized by Our World in Data [26].

Methodologically, we exploit a structural property of the task. In logarithms, the Kaya identity [27,28] renders per-capita emissions approximately linear in energy intensity and carbon intensity, which explains an empirical result we report below: a ridge regression is remarkably hard to beat. Rather than ignoring this, we encode it. The proposed KG-CBA network attaches a log-linear head, initialized at a ridge solution, to a convolutional, bidirectional-recurrent, attention-pooled branch that learns only the nonlinear residual, tuned by particle swarm optimization [29-31]. Uncertainty is quantified with Monte-Carlo dropout [32] calibrated by per-fold split-conformal inference [33-35], and interpretability through SHapley Additive exPlanations [36] and attention-weight analysis.

The contributions are fivefold, and are as much about how the evidence is established as about what it shows. (i) A rigorously country-disjoint, 112-country LOCO benchmark of thirteen statistical, machine-learning, and deep-learning models on open, measured data, with country-clustered significance testing throughout. (ii) A physics-guided hybrid architecture, KG-CBA, with PSO-based hyperparameter optimization, which significantly improves its unguided counterpart. (iii) An interpretable error decomposition showing that a handful of structurally atypical energy systems dominates the error budget, and that a single additional covariate roughly halves median estimation error where it is available. (iv) Distribution-aware uncertainty quantification whose honest coverage shortfall is traced to non-exchangeability under grouped resampling. (v) A temporal experiment showing that naive persistence is a strong benchmark whose margin over well-specified learners is small and unstable across evaluation windows.

Section 2 reviews related work. Section 3 describes the data and methods. Section 4 reports results. Section 5 discusses implications, limitations, and threats to validity. Section 6 concludes.

2. Related work

2.1 Machine and deep learning for CO_2 emission modelling

Comparative studies consistently find nonlinear learners competitive or superior to classical statistical models for emission prediction. Ajala et al. [11] benchmarked statistical (ARMA/ARIMA family), machine-learning (SVM, random forest, gradient boosting), and seven deep architectures for daily CO_2 across China, India, the USA, and Europe. Architecture-comparison studies report horizon-dependent trade-offs among LSTM, GRU, CNN-LSTM, and dense networks [12], while temporal convolutional hybrids with hyper parameter search achieve strong accuracy on periodic emission series [13]. Attention-augmented and feature-fused hybrids continue this trend: CNN-BiLSTM-attention frameworks improve daily national and plant-level carbon prediction [14,15], and TCN-LSTM hybrids transfer to maritime emissions [16]. Sector-specific applications include transport [17,37-39], data centers [40], and energy-based national totals [41]. Marked publication emphasis on incremental architecture novelty, however, has not been matched by equally careful evaluation design, motivating the protocol adopted here.

2.2 Emissions modelling for data-sparse regions

For Africa specifically, ensemble tree methods have been applied to building-sector emissions across six nations [7], continent-wide emission determinants for 48 countries [8], carbon-neutrality trajectories in sub-Saharan Africa [9], and transport emissions of the continent's four largest emitters [10]; a national decarburization-planning framework has been proposed for Nigeria [42]. Beyond Africa, machine-learning gap-filling of subnational inventories demonstrates the feasibility of covariate-based estimation at scale [6]. Inventory-quality assessments document why such estimation is needed: most non-Annex I countries rely on Tier-1 approaches with scarce activity data, and independent datasets disagree most where capacity is lowest [3-5,43]. Our LOCO formulation directly simulates this deployment setting, which, to our knowledge, has not previously been used to benchmark hybrid deep architectures at global scale.

2.3 Metaheuristic optimization, uncertainty, and explainability

Metaheuristic hyper parameter tuning is now standard practice in energy and emissions forecasting: PSO variants improve LSTM load forecasting [19,44], attention-augmented CNN-LSTM demand models [20], and bidirectional recurrent emission predictors, while novel hybrids have been applied directly to CO_2 prediction [21]. For uncertainty, conformal prediction supplies distribution-free finite-sample coverage [33,45]; ensemble conformalized quantile regression extends it to probabilistic time series [34], with energy-domain applications in solar forecasting [46,47], and recent theory characterizes behavior under non-exchangeable data [35,48], directly relevant to our grouped country splits. For explainability, SHAP [36] is the de-facto standard in emission applications [49-51]. The present study integrates all three strands within a single, reproducible pipeline.

2.4 The gap this study fills

Table B3 positions this work against representative prior studies on five axes. To our knowledge, no previous study of machine learning for national CO_2 estimation combines all of the following: (i) evaluation under strictly country-disjoint splits, so that no test country contributes any training signal; (ii) explicit naive benchmarks with scaled error, so that reported skill is measured against the persistence a random walk would deliver; (iii) inference clustered at the country level, so that repeated years within a country are not counted as independent evidence; (iv) architectural structure derived from an accounting identity rather than chosen by search; and (v) distribution-free uncertainty quantification reported honestly under the grouped sampling the task requires. Individually each of these is established practice in some adjacent literature. Their absence in combination is what allows the field's reported accuracies to look far better than they generalize, and supplying them in combination is this paper's principal methodological contribution. The substantive contribution follows from it: once the evaluation is trustworthy, the ranking of what actually improves national emission estimation changes, and the binding constraint turns out to be data availability in specific countries rather than model capacity.

3. Materials and methods

3.1 Data sources and panel construction

All measured series derive from Our World in Data's harmonized CO_2 and energy datasets [26], which redistribute the Global Carbon Budget national emission accounts [2] and the Energy Institute Statistical Review primary-energy statistics [25], accessed 26 July 2026. From the raw country-year records we retain 1990-2023 and exclude regional aggregates. Six covariates form the core feature set: primary energy consumption per capita E_t (kWh person^{-1}), GDP per capita G_t (constant international-\$), population P_t, and the coal, oil, and gas shares of CO_2, $s_t^{coal} = \text{coal}\, CO_2/CO_2$ and analogously for oil and gas. The target is per-capita fossil CO_2, c_t (t CO_2 person^{-1} yr^{-1}).

Interior gaps of at most three consecutive years are filled by linear interpolation; series edges are extended with the nearest observed value. Countries are retained if all seven series are complete for all 34 years after this treatment, yielding a balanced panel of 112 countries × 34 years (3,808 country-years); the ISO codes of the retained economies are listed in Table B4.

Imputation is material and unevenly distributed, and we report it in full. Table 3 gives the audit. Population, oil share and per-capita CO_2 require no filling; energy per capita is filled for 0.7% of country-years and GDP per capita for 3.0%, but the coal and gas shares are filled for 6.4% and 7.6% respectively. Critically, because the edge rule carries no length cap, some series are extended over long stretches: the longest single filled run reaches 31 years for the gas share, 26 for the coal share and 16 for energy per capita. Twenty-five of the 112 countries contain at least one filled run exceeding three years, and nineteen contain a run exceeding ten; Table B5 lists the twelve longest. These countries are disproportionately low- and middle-income (El Salvador 31 years, Niger 29, Panama 28, Ghana 26, Jamaica 26, Guatemala 26, Cameroon 26, Rwanda 25, Benin 24), because it is precisely there that the international energy lineages are thin. Constant extension makes a covariate series artificially smooth and therefore artificially easy to predict from, so this imputation flatters rather than penalizes the affected countries; Section 4.4 quantifies the effect and Section 5.3 discusses it. All country-level results below are annotated with imputation status, and the full per-country audit is released with the code.

The panel spans 0.03-364.8 t CO_2 person^{-1} over 1990-2023. Because the eight-year window means prediction targets run 1997-2023, the largest *modelled* value is Qatar's 76.7 t person^{-1} in 1997; Kuwait's 1991 value of 364.8 t person^{-1}, a genuine artefact of the Gulf-War oil fires coinciding with a population collapse, enters only as covariate context and is never a prediction target.

For Experiment C, a seventh covariate, the low-carbon share of primary energy s_t^{lc} (renewables plus nuclear), available from the Statistical Review lineage for 76 of the 112 countries (≥90% completeness), is added under identical processing with no additional imputation required. This sub-panel contains all the countries later identified as error-dominating outliers.

3.2 Problem formulation

Let i index countries and t years. Skewed magnitudes are log-transformed via equation (1),

$$e_{i,t} = \log_{10} E_{i,t}, \qquad g_{i,t} = \log_{10} G_{i,t}, \qquad p_{i,t} = \log_{10} P_{i,t} \tag{1}$$

and the target is modelled in natural logarithm, equation (2),

$$y_{i,t} = \ln c_{i,t}. \tag{2}$$

For each country-year with at least W years of history we form the covariate window of equation (3),

$$\mathbf{X}_{i,t} = [\mathbf{x}_{i,t-W+1},\dots,\mathbf{x}_{i,t}] \in \mathbb{R}^{W\times F}, \qquad \mathbf{x}_{i,\tau} = \left(e_{i,\tau}, g_{i,\tau}, p_{i,\tau}, s^{coal}_{i,\tau}, s^{oil}_{i,\tau}, s^{gas}_{i,\tau}\right) \qquad (3)$$

with $W = 8$ and $F = 6$ ($F = 7$ in Experiment C), giving 3,024 samples (2,052 in Experiment C). The LOCO task is to learn f such that $\hat{y}_{i,t} = f(\mathbf{X}_{i,t})$ generalizes to countries absent from training. Evaluation uses grouped five-fold cross-validation with countries as groups, so the test country's entire target series is invisible during training; features are standardized per fold as in equation (4),

$$\tilde{\mathbf{X}} = (\mathbf{X} - \boldsymbol{\mu}_{tr}) \;/\; \boldsymbol{\sigma}_{tr}, \qquad (4)$$

with $\boldsymbol{\mu}_{tr}, \boldsymbol{\sigma}_{tr}$ computed on training folds only. Within each training fold, one-seventh of the *countries* form an inner validation set for early stopping and hyperparameter selection, preserving country-disjointness at every level.

Scope of the "no own emissions" claim. The target country's emission *history* is withheld by construction, and no lagged value of c enters the feature set. The three fuel-share covariates are, however, ratios computed from that country's own CO_2 accounts, s^{coal} = coal CO_2/CO_2 and so on. They reveal no information about the *level* of emissions, which is the estimand, but they are not obtainable from a country that has no emission accounts at all; in a genuine deployment they would be derived from national energy balances instead. The task therefore simulates a country whose *fuel mix* is characterized but whose *emission level* is not. Section 4.2 reports a covariate ablation that removes the fuel shares entirely; it shows their contribution is under one percentage point of median error, so the distinction is minor in practice. Section 5.3 returns to the point.

3.3 Kaya-motivated linear backbone

The Kaya identity decomposes national emissions as $C = P \cdot (G/P) \cdot (E/G) \cdot (C/E)$ [27,28]. Dividing by population and taking logarithms yields equation (5),

$$\ln c = \ln \frac{E}{P} + \ln \frac{C}{E}, \tag{5}$$

i.e., log per-capita emissions equal log per-capita energy plus log carbon intensity of energy. Because carbon intensity is, to first order, a mixture over fuel shares, equation (5) implies that a linear model in $(e, g, p, s^{coal}, s^{oil}, s^{gas})$ should capture the bulk of cross-country variance, an implication our results confirm.

Two ridge estimators appear in this paper and must be distinguished. The **benchmark ridge** of Table 1 is fitted on the flattened window $\mathrm{vec}(\tilde{\mathbf{X}}) \in \mathbb{R}^{WF}$, equation (6),

$$\hat{\boldsymbol{\beta}} = \operatorname*{argmin}_{\boldsymbol{\beta}} \sum_{n} (y_n - \boldsymbol{\beta}^\top \mathrm{vec}(\tilde{\mathbf{X}}_n))^2 + \lambda \parallel \boldsymbol{\beta} \parallel_2^2, \qquad \lambda = 1. \tag{6}$$

The **warm-start ridge** used to initialize the hybrid's linear head (Section 3.5) is the more parsimonious variant fitted on the most recent window step $\tilde{\mathbf{x}}_{n,W} \in \mathbb{R}^F$ alone, so that the head has one weight per covariate. Fitted on the last step, ridge attains RMSE 3.343 and R^2 0.761 in LOCO; fitted on the full window, RMSE 3.056 and R^2 0.800. Table 1 reports the latter.

3.4 Benchmark models

Thirteen models are compared under identical folds and inputs: a training-set mean predictor; ridge regression (6); k-nearest neighbours (k = 7, distance-weighted); support vector regression (RBF kernel, C = 10, ε = 0.01); random forest (600 trees, depth ≤ 14); XGBoost [52] (800 trees, η = 0.03, depth 6, subsample 0.85); LightGBM [53] (800 trees, η = 0.03, 63 leaves, subsample 0.85, colsample 0.85, L2 penalty 1.5); LSTM; GRU; CNN-LSTM; CNN-BiLSTM-Attention; and the two proposed hybrids KG-CBA and PSO-KG-CBA. Classical learners operate on the flattened window $\mathrm{vec}(\tilde{\mathbf{X}})$; deep sequence models consume $\tilde{\mathbf{X}}$ directly. The LSTM cell [54] is given by equations (7)-(12):

$$\mathbf{f}_\tau = \sigma\left(\mathbf{W}_f\mathbf{x}_\tau + \mathbf{U}_f\mathbf{h}_{\tau-1} + \mathbf{b}_f\right) \tag{7}$$

$$\mathbf{i}_\tau = \sigma(\mathbf{W}_i\mathbf{x}_\tau + \mathbf{U}_i\mathbf{h}_{\tau-1} + \mathbf{b}_i) \tag{8}$$

$$\mathbf{o}_\tau = \sigma(\mathbf{W}_o\mathbf{x}_\tau + \mathbf{U}_o\mathbf{h}_{\tau-1} + \mathbf{b}_o) \tag{9}$$

$$\tilde{\mathbf{c}}_\tau = \tanh(\mathbf{W}_c\mathbf{x}_\tau + \mathbf{U}_c\mathbf{h}_{\tau-1} + \mathbf{b}_c) \tag{10}$$

$$\mathbf{c}_\tau = \mathbf{f}_\tau \odot \mathbf{c}_{\tau-1} + \mathbf{i}_\tau \odot \tilde{\mathbf{c}}_\tau \tag{11}$$

$$\mathbf{h}_\tau = \mathbf{o}_\tau \odot \tanh(\mathbf{c}_\tau) \tag{12}$$

with σ the logistic function and $\odot$ the Hadamard product. The GRU uses update and reset gates, equations (13)-(15),

$$\mathbf{z}_\tau = \sigma(\mathbf{W}_z\mathbf{x}_\tau + \mathbf{U}_z\mathbf{h}_{\tau-1} + \mathbf{b}_z) \tag{13}$$

$$\mathbf{r}_\tau = \sigma(\mathbf{W}_r\mathbf{x}_\tau + \mathbf{U}_r\mathbf{h}_{\tau-1} + \mathbf{b}_r) \tag{14}$$

$$\mathbf{h}_\tau = (1 - \mathbf{z}_\tau) \odot \mathbf{h}_{\tau-1} + \mathbf{z}_\tau \odot \tanh(\mathbf{W}_h\mathbf{x}_\tau + \mathbf{U}_h(\mathbf{r}_\tau \odot \mathbf{h}_{\tau-1}) + \mathbf{b}_h). \tag{15}$$

The CNN-LSTM stacks two one-dimensional convolutions, equation (16),

$$\mathbf{z}_\tau^{(l)} = \mathrm{ReLU}\left(\sum_{j=1}^{k} \mathbf{K}_j^{(l)}\, \mathbf{z}_{\tau+j-\lceil k/2\rceil}^{(l-1)} + \mathbf{b}^{(l)}\right), \tag{16}$$

before an LSTM encoder. All fixed deep baselines use 48 filters/units, kernel 3, dropout 0.25, Adam (10^{-3}), batch 96, ≤90 epochs with early stopping (patience 9) on the inner country-disjoint validation loss of equation (17),

$$\mathcal{L} = \frac{1}{N}\sum_{n}(y_n - \hat{y}_n)^2. \tag{17}$$

3.5 Kaya-guided CNN-BiLSTM-Attention (KG-CBA)

The proposed architecture decomposes the prediction into a physics-guided linear term and a learned residual, equation (18):

$$\hat{y} = \underbrace{\boldsymbol{\beta}^{\top}\tilde{\mathbf{x}}_W + \beta_0}_{\text{Kaya head}} + \underbrace{r_{\boldsymbol{\theta}}(\tilde{\mathbf{X}})}_{\text{deep residual branch}}. \tag{18}$$

The Kaya head is a single dense unit acting on the most recent window step, *warm-started* at the fold-specific last-step ridge solution (Section 3.3) and refined jointly during training. The residual branch applies two Conv1D layers (16), a bidirectional LSTM whose forward and backward states are concatenated in equation (19),

$$\mathbf{h}_\tau = \left[\overrightarrow{\mathbf{h}}_\tau \,\|\, \overleftarrow{\mathbf{h}}_\tau\right], \tag{19}$$

and additive temporal attention [55] that pools the sequence into a context vector through equations (20)-(22),

$$u_\tau = \mathbf{v}^{\top}\tanh(\mathbf{W}_a\mathbf{h}_\tau + \mathbf{b}_a) \tag{20}$$

$$\alpha_\tau = \frac{\exp(u_\tau)}{\sum_{\tau'=1}^{W}\exp(u_{\tau'})} \tag{21}$$

$$\mathbf{s} = \sum_{\tau=1}^{W} \alpha_\tau \, \mathbf{h}_\tau, \tag{22}$$

followed by a 32-unit dense layer, dropout, and a linear residual output whose kernel is initialized near zero so that training starts from the ridge solution. This design lets gradient descent spend capacity only where the log-linear Kaya approximation fails.

3.6 Particle swarm optimization of the hybrid

Six hyperparameters are tuned: convolution filters $\in [16,64]$, kernel size $\in \{2,3,4\}$, BiLSTM units $\in [16,96]$, dropout $\in [0.05,0.45]$, learning rate $\in [2 \times 10^{-4}, 3 \times 10^{-3}]$ (log-scale), and batch size $\in \{48,64,96,128\}$. PSO [29] evolves six particles for five iterations (30 evaluations). Particle j updates according to equations (23)-(24) as

$$\mathbf{v}_j \leftarrow \omega \mathbf{v}_j + c_1 \mathbf{r}_1 \odot \left(\mathbf{p}_j^{best} - \mathbf{p}_j\right) + c_2 \mathbf{r}_2 \odot \left(\mathbf{g}^{best} - \mathbf{p}_j\right) \tag{23}$$

$$\mathbf{p}_j \leftarrow \mathrm{clip}\left(\mathbf{p}_j + \mathbf{v}_j, \, \mathbf{l}, \mathbf{u}\right) \tag{24}$$

with inertia $\omega = 0.7$, cognitive and social constants $c_1 = c_2 = 1.5$, $\mathbf{r}_1, \mathbf{r}_2 \sim \mathcal{U}(0,1)^6$, velocities clamped to 30% of each range, and fitness defined as inner-validation MSE on a country-disjoint split of the first training fold. The converged configuration (37 filters, kernel 4, 40 units, dropout 0.231, learning rate 9.96×10^{-4}, batch 48; validation MSE 0.0522) is retrained on all five folds, denoted PSO-KG-CBA (E-PSO-KG-CBA on the enriched panel). Table B1 reports the full search space alongside the converged values.

3.7 Uncertainty quantification: conformalized Monte-Carlo dropout

Epistemic uncertainty is estimated by Monte-Carlo dropout [32]: with dropout active at inference, $T = 60$ stochastic forward passes yield the predictive moments of equation (25),

$$\bar{y}(\mathbf{X}) = \frac{1}{T}\sum_{s=1}^{T} \hat{y}^{(s)}(\mathbf{X}), \qquad \hat{\sigma}^2(\mathbf{X}) = \frac{1}{T}\sum_{s=1}^{T} (\hat{y}^{(s)}(\mathbf{X}) - \bar{y}(\mathbf{X}))^2. \tag{25}$$

Because raw MC-dropout intervals are severely over-confident, we calibrate them per fold by split-conformal inference [33,34]: on each fold's country-disjoint inner validation set, normalized nonconformity scores, equation (26),

$$s_n = \frac{|y_n - \bar{y}(\mathbf{X}_n)|}{\hat{\sigma}(\mathbf{X}_n)} \tag{26}$$

are computed, the level-adjusted quantile $\hat{q} = s_{(\lceil 0.9(n_{cal}+1)\rceil)}$ is extracted, and the test-fold interval, equation (27), is

$$[\exp(\bar{y} - \hat{q}\hat{\sigma}), \exp(\bar{y} + \hat{q}\hat{\sigma})]. \tag{27}$$

Coverage validity assumes exchangeability between calibration and test units [35,48]; grouped country sampling violates this, and Section 4.5 quantifies the resulting shortfall rather than concealing it.

3.8 Explainability

Global attributions use SHAP [36]. For a tree ensemble f and feature j, the attribution is given by equation (28),

$$\phi_j = \sum_{S \subseteq \mathcal{F}\setminus\{j\}} \frac{|S|!\,(|\mathcal{F}| - |S| - 1)!}{|\mathcal{F}|!} [f(S \cup \{j\}) - f(S)], \tag{28}$$

computed exactly via TreeExplainer on the enriched LightGBM and aggregated over the 56 window columns by covariate and by lag. Because the flattened design matrix is lag-major (column index $= \tau \cdot F + j$), the attribution array is reshaped to (N, W, F) before aggregation; aggregating under the transposed layout silently interchanges covariates and lags. Temporal importance of the hybrid is read directly from the learned attention weights α_τ in (21).

3.9 Evaluation metrics and clustered statistical testing

With observed c_n and predicted $\hat{c}_n = \exp(\hat{y}_n)$ on the raw scale, accuracy is scored by equations (29)-(33);

$$\mathrm{RMSE} = \sqrt{1/N \sum_n (c_n - \hat{c}_n)^2} \tag{29}$$

$$\mathrm{MAE} = 1/N \sum_n |c_n - \hat{c}_n| \tag{30}$$

$$\mathrm{MAPE} = 100/N \sum_n |c_n - \hat{c}_n / c_n| \tag{31}$$

$$\mathrm{MdAPE} = 100 \cdot \mathrm{median}_n |c_n - \hat{c}_n / c_n| \tag{32}$$

$$R^2 = 1 - \frac{\sum_n (c_n - \hat{c}_n)^2}{\sum_n (c_n - \bar{c})^2}. \tag{33}$$

For the temporal experiment, the mean absolute scaled error against the in-sample naive forecast [22], equation (34),

$$\mathrm{MASE}_h = \frac{\frac{1}{N} \sum_n |c_n - \hat{c}_n|}{\frac{1}{T_{tr} - h} \sum_{t=h+1}^{T_{tr}} |c_t - c_{t-h}|}, \tag{34}$$

flags genuine skill (MASE < 1); the denominator is computed per country on the training period, so each country's errors are scaled by its own naive difficulty. Because the denominator is in-sample while the numerator is out-of-sample, persistence itself need not attain MASE = 1: it scores 1.198 at h = 1 in the 2021-2023 window, reflecting genuinely higher post-2020 volatility, and 0.995 in the pre-pandemic replication.

Clustered inference. The out-of-fold sample contains 27 repeated years for each of 112 countries, so country-years are far from independent. We therefore report three quantities for every model pair: a paired Wilcoxon signed-rank test on absolute percentage error at the observation level (the conventional but anticonservative test, retained only for comparison); a paired Wilcoxon test on *per-country median* APE, with $n = 112$ clusters; and a cluster bootstrap that resamples **countries** with replacement (10,000 draws) to obtain a 95% confidence interval and two-sided p-value for the difference in pooled median APE. Conclusions are drawn from the clustered tests. Software: Python 3.12.3, TensorFlow 2.21.0 (CPU), XGBoost 3.4.0, LightGBM 4.7.0, scikit-learn 1.8.0, SHAP 0.52.0; global seed 42 with per-fold offsets.

3.10 Experiment B: temporal forecasting protocol

To situate the LOCO results against conventional forecasting, we recast the panel as an h-step-ahead task in which the target country's own emission history *is* available, so that persistence is well defined. Predictors are the eight-year window of the six covariates augmented with the country's own lagged log emissions (56 columns); withholding the latter would handicap the learners relative to persistence and make the comparison uninformative. Targets are formed in two ways: a *level* formulation predicting y_{t+h} directly, and a *log-growth* formulation predicting $y_{t+h} - y_t$. Models are trained on all pairs with $t + h \leq 2017$ and tested on target years 2021-

2023, with a pre-pandemic replication trained through 2012 and tested on 2015-2019. Baselines are persistence, $\hat{c}_{t+h} = c_t$, and drift, $\hat{y}_{t+h} = y_t + h\bar{\Delta}_3$ with $\bar{\Delta}_3$ the mean of the last three log-changes. Six learners are evaluated under each formulation, and each learner is compared against persistence by a cluster bootstrap over countries.

4. Results

4.1 Panel characteristics

Figure 1 summarizes the panel: mean per-capita emissions decline gently after 2007 while trajectories diverge. Figure 2 confirms the Kaya expectation: ln CO_2pc correlates at r = 0.93 with log energy per capita and r = 0.82 with log GDP per capita, while fuel shares carry weaker marginal correlations. Continental distributions (Figure 3) span three orders of magnitude. The framework is depicted in Figure 4 and the KG-CBA architecture in Figure 5.

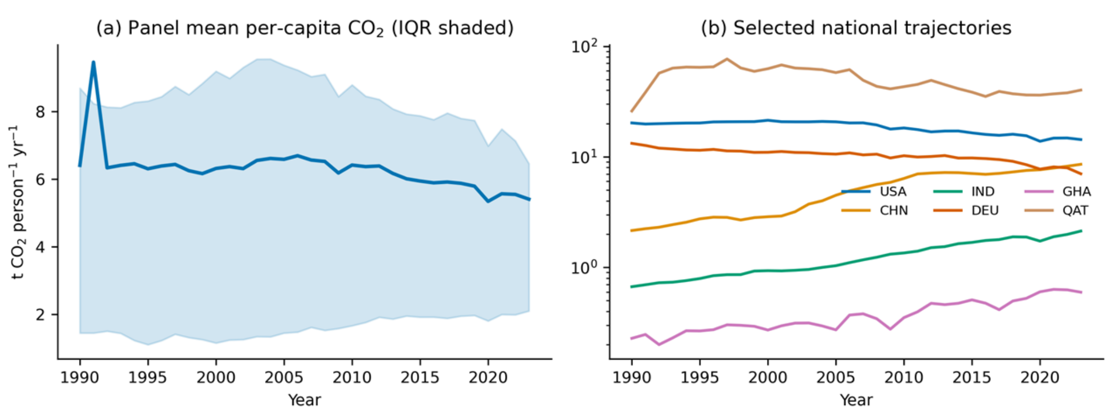

Figure 1. *Per-capita CO2 in the 112-country panel, 1990-2023: (a) panel mean with interquartile range; (b) selected national trajectories (log scale).*

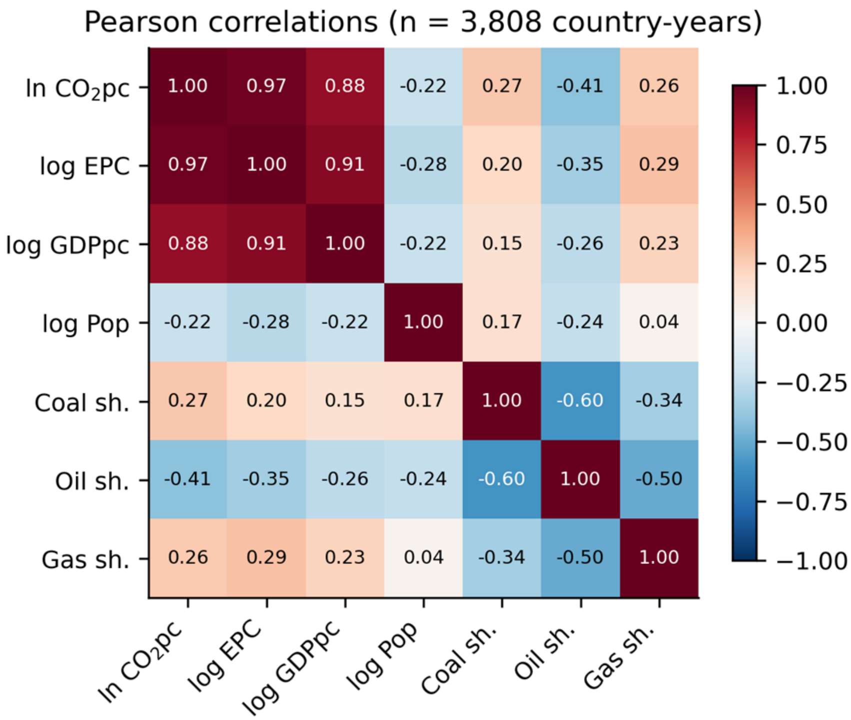

Figure 2. Pearson correlation matrix of the log-transformed target and the six core covariates (3,808 country-years).

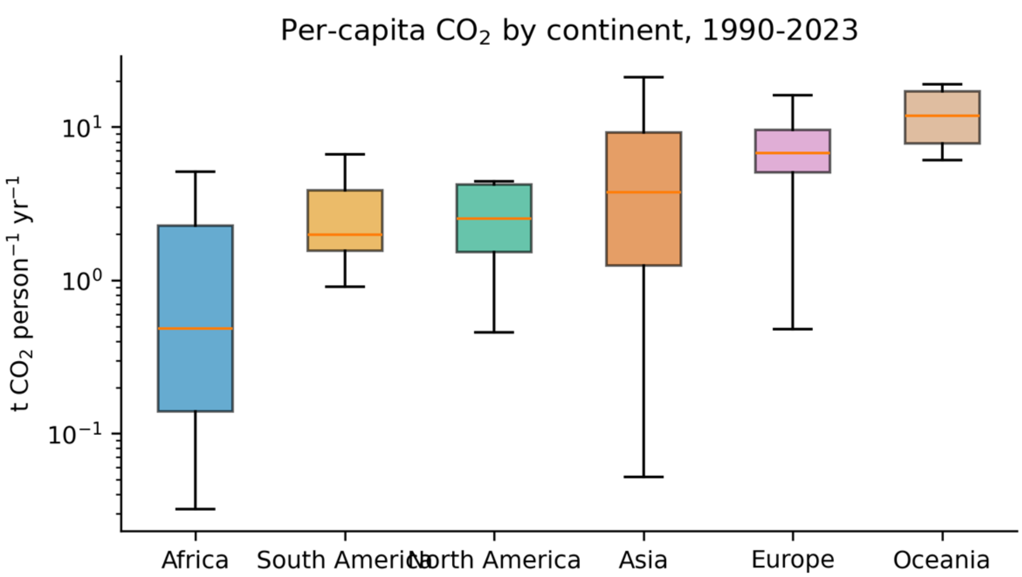

Figure 3. *Distribution of per-capita CO2 by continent (log scale).*

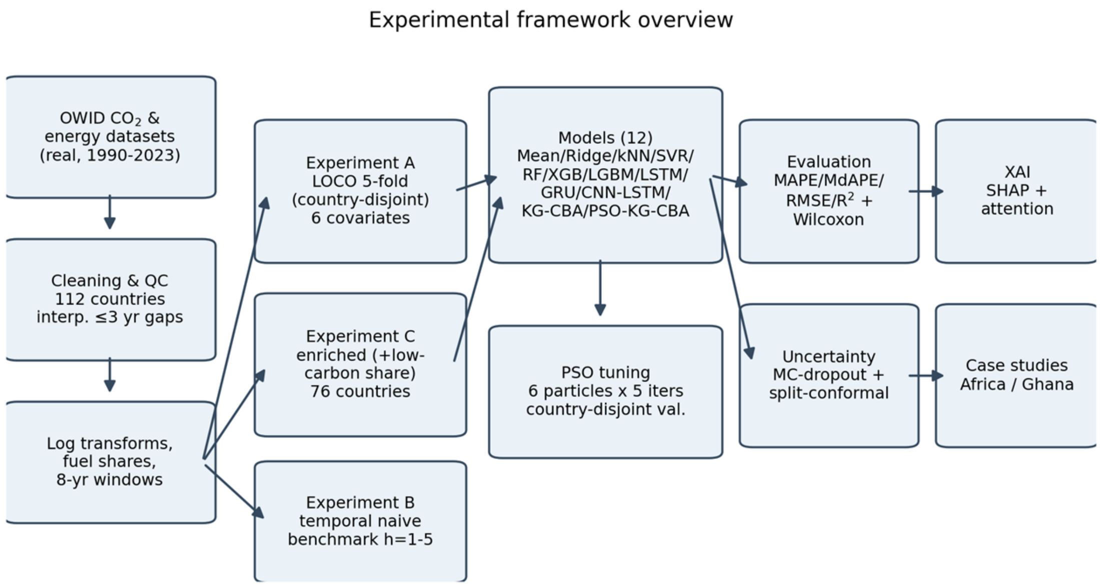

__Figure 4.__ Overview of the experimental framework.

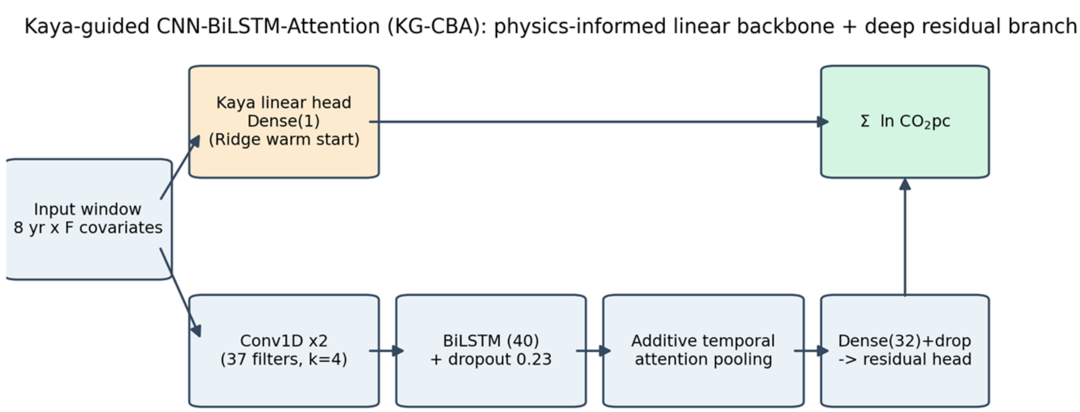

__Figure 5.__ The Kaya-guided CNN-BiLSTM-Attention (KG-CBA) architecture.

4.2 Experiment A: 112-country LOCO benchmark

Two diagnostics confirm that tuning and training behaved as intended. The PSO fitness trace converges well inside the 30-evaluation budget: the global-best inner-validation MSE improves in four steps from 0.0645 to 0.0522 and is unchanged over the final fourteen evaluations (Figure 6). Fold-1 learning curves for the four fixed deep baselines show training and inner-validation loss falling together, with early stopping halting each run between roughly twelve and forty epochs, well short of the 90-epoch cap, and no upward drift in validation loss thereafter (Figure 7).

Table 1 reports out-of-fold accuracy for all thirteen models plus the ensemble; Figure 8 shows the comparison and Figure 9 predicted-observed agreement across four orders of magnitude.

Three patterns stand out. First, the task is learnable but hard: the mean predictor fails catastrophically (MAPE 337.8%), whereas every covariate-using learner achieves MAPE below 50%. Second, the Kaya mechanism dominates. Ridge regression, linear in log space, attains R^2 = 0.800 and MdAPE 16.3%, outperforming every tree ensemble and every unguided deep network, including the plain CNN-BiLSTM-Attention (MdAPE 20.8%); both gaps survive country-clustered testing (ridge vs LightGBM $p = 0.006$; ridge vs CNN-BiLSTM-Attention $p = 0.002$). Third, physics guidance closes the gap from the deep side: adding the Kaya head lifts the hybrid's MdAPE from 20.8% to 15.7%, and both KG-CBA and PSO-KG-CBA significantly outperform the unguided architecture under clustering ($p = 0.002$ for each).

The ensemble's advantage over ridge does not survive clustered inference. Table 2 contrasts the two testing regimes. Averaging ridge, GRU and PSO-KG-CBA gives the best point accuracy in the study (MAPE 23.5%, MdAPE 15.1%), and an observation-level Wilcoxon test returns $p = 7 \times 10^{-10}$ against ridge. But the per-country test gives $p = 0.098$ and the cluster bootstrap $p = 0.22$, with a 95% interval for the median-APE difference of [-2.20, +0.41] percentage points that comfortably spans zero. We therefore claim no significant improvement of the ensemble over ridge alone. The ensemble does significantly beat GRU ($p = 0.0006$) and the PSO-tuned hybrid ($p = 0.022$), so the gain is real relative to the deep constituents and illusory relative to the linear one. The composition of the ensemble was chosen after inspecting out-of-fold performance and is therefore not the product of a protected selection procedure; this is a further reason to treat its margin cautiously. Per-fold results reinforce the caution: across the five folds the ensemble's MdAPE ranges from 10.1% to 25.6% and the ranking of the leading models is not stable (Table B2), so a single pooled comparison overstates the precision with which the leading models can be separated.

Covariate ablation. Because three of the six covariates are ratios derived from the target country's own CO_2 accounts (Section 3.2), we retrained ridge without them. Using only energy per capita, GDP per capita and population, MdAPE rises from 16.3% to 16.9% and R^2 falls from 0.800 to 0.775; using log energy per capita alone, MdAPE is 17.9% and R^2 0.723 (Table B6). The fuel shares are therefore worth well under one percentage point of median error. Essentially all of the achievable LOCO accuracy is obtainable from energy-economic covariates that carry no emission-account provenance whatsoever, so the estimator is deployable for a country with no inventory of any kind.

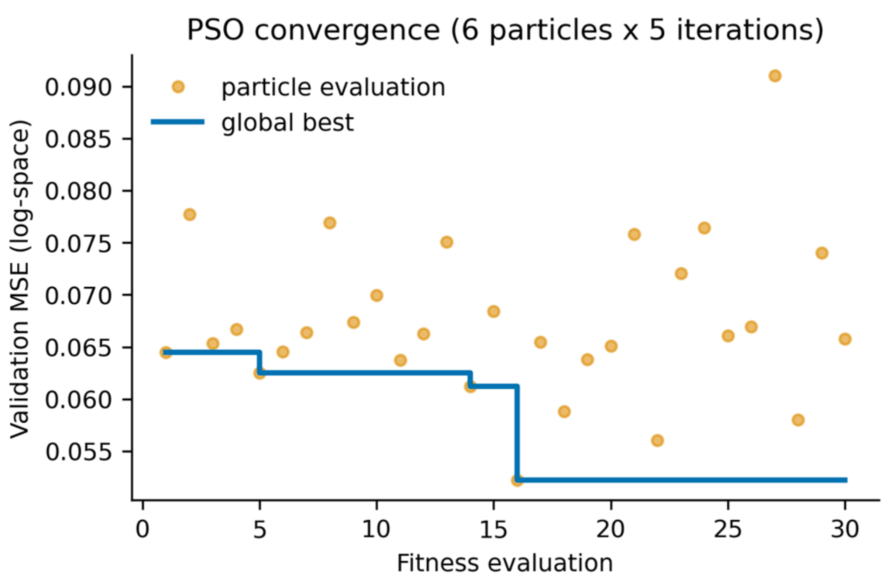

Figure 6. *PSO convergence over 30 fitness evaluations. (Supplementary)*

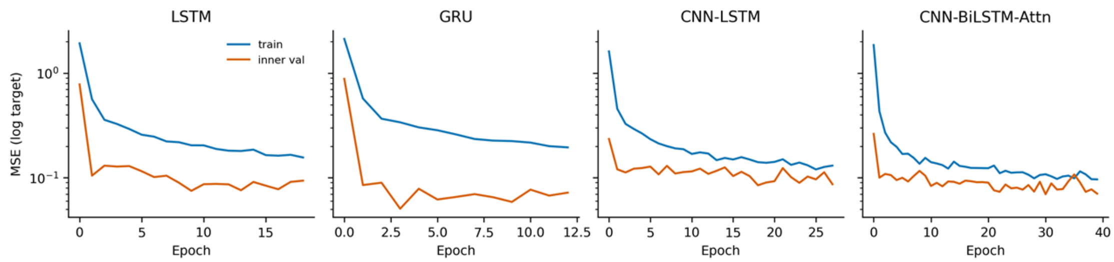

Figure 7. Fold-1 training dynamics of the four fixed deep baselines. (Supplementary)

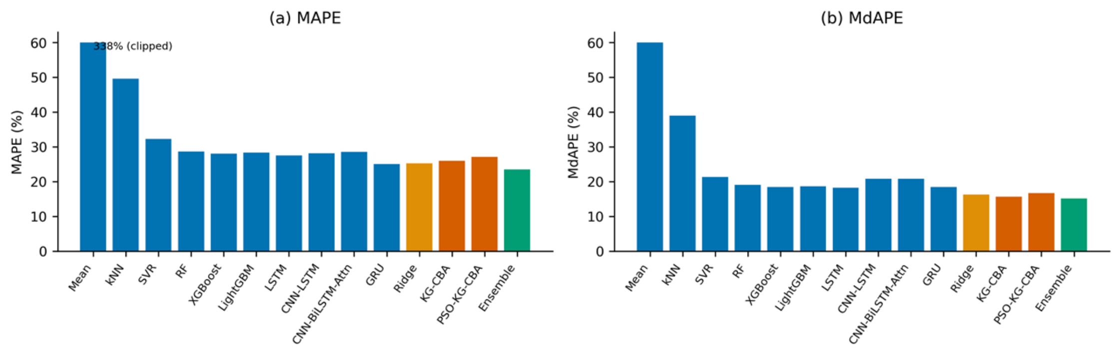

Figure 8. *Experiment A leave-country-out error by model.*

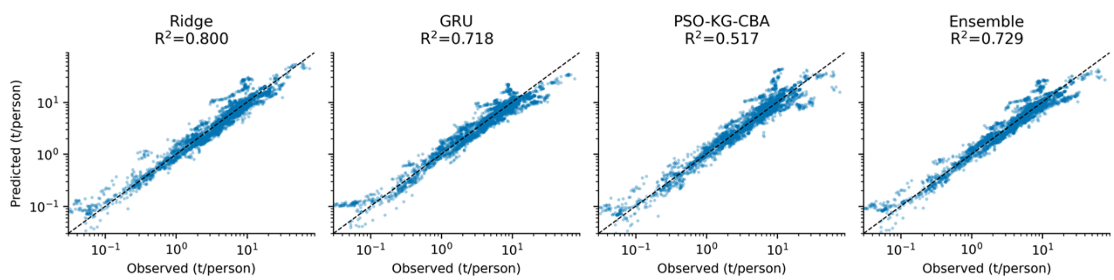

Figure 9. *Out-of-fold predicted versus observed per-capita CO2 (log-log).*

Table 1. Out-of-fold LOCO performance, Experiment A (112 countries, 6 covariates).

Model	RMSE	MAE	MAPE (%)	MdAPE (%)	R^2
Mean	7.415	4.408	337.8	63.3	−0.178
kNN	5.119	2.729	49.7	39.0	0.439

Model	RMSE	MAE	MAPE (%)	MdAPE (%)	R^2
SVR	4.881	2.100	32.3	21.3	0.490
Random forest	4.233	1.824	28.7	19.1	0.616
XGBoost	4.043	1.775	28.0	18.4	0.650
LightGBM	3.943	1.813	28.4	18.6	0.667
LSTM	3.815	1.703	27.6	18.2	0.688
CNN-LSTM	3.773	1.707	28.1	20.8	0.695
CNN-BiLSTM-Attn	3.812	1.790	28.6	20.8	0.689
GRU	3.629	1.644	25.1	18.5	0.718
Ridge (Kaya log-linear)	**3.056**	**1.443**	25.2	16.3	**0.800**
KG-CBA (ours)	4.595	1.898	26.0	**15.7**	0.548
PSO-KG-CBA (ours)	4.748	1.914	27.2	16.7	0.517
Ensemble (Ridge + GRU + PSO-KG-CBA)	3.557	1.530	**23.5**	15.1	0.729

Table 2. Observation-level versus country-clustered inference on paired absolute percentage error. Δ is the difference in pooled median APE (percentage points); the interval is a 95% cluster bootstrap over countries (10,000 draws). Conclusions follow the clustered columns.

Experiment	Comparison	MdAPE A / B (%)	p (observation-level)	p (per-country)	Δ [95% CI]	p (cluster bootstrap)	Conclusion

Experiment	Comparison	MdAPE A / B (%)	p (observation-level)	p (per-country)	Δ [95% CI]	p (cluster bootstrap)	Conclusion
A	Ensemble vs Ridge	15.1 / 16.3	6.9×10^{-10}	0.098	−0.76 [−2.20, +0.41]	0.22	not significant
A	Ensemble vs GRU	15.1 / 18.5	1.8×10^{-30}	0.007	−2.57 [−3.77, −1.20]	0.0006	significant
A	Ensemble vs PSO-KG-CBA	15.1 / 16.7	3.6×10^{-31}	0.074	−1.33 [−2.85, −0.22]	0.022	significant
A	PSO-KG-CBA vs CNN-BiLSTM-Attn	16.7 / 20.8	6.3×10^{-22}	0.004	−3.51 [−5.97, −0.97]	0.0016	significant
A	KG-CBA vs CNN-	15.7 / 20.8	4.9×10^{-26}	0.004	−3.42 [−5.84	0.0018	significant

Experiment	Comparison	MdAPE A / B (%)	p (observation-level)	p (per-country)	Δ [95% CI]	p (cluster bootstrap)	Conclusion
	BiLSTM-Attn				, −1.21]		
A	Ridge vs LightGBM	16.3 / 18.6	8.3×10^{-25}	0.026	−3.10 [−4.91, −1.03]	0.0058	significant
A	Ridge vs CNN-BiLSTM-Attn	16.3 / 20.8	3.1×10^{-34}	0.007	−4.29 [−7.05, −1.64]	0.0024	significant
C	Ensemble vs Ridge	7.35 / 7.72	0.483	0.491	−0.20 [−0.66, +0.36]	0.56	not significant
C	E-PSO-KG-CBA vs LightGBM	8.09 / 13.10	1.7×10^{-56}	0.0002	−3.85 [−6.03, −1.95]	0.0001	significant
C	Ensemble	7.35 /	5.1×10^{-31}	0.004	−0.86	0.0014	significant

Experiment	Comparison	MdAPE A / B (%)	p (observation-level)	p (per-country)	Δ [95% CI]	p (cluster bootstrap)	Conclusion
	vs E-PSO-KG-CBA	8.09			[−1.45, −0.35]		

4.3 Error anatomy and the covariate-availability effect (Experiment C)

A Pareto decomposition of squared error (Figure 10) reveals extreme concentration: the six worst-fitting economies contribute 79.3% of the ensemble's total squared error and 84.3% for the hybrid alone. The *composition* of that group is only partly stable across models. Singapore, Qatar and Kuwait appear in the top six under all six models examined; Iceland, Norway, Luxembourg and Saudi Arabia exchange places depending on the estimator. What the group shares is structural: hydro- and geothermal-dominant grids (Norway, Iceland), hydrocarbon-exporting states (Qatar, Kuwait, Saudi Arabia), and city-states with bunker-fuel and finance-driven energy profiles (Singapore, Luxembourg). The residuals, in other words, *locate the failure of the Kaya carbon-intensity proxy*, and the identity of the specific worst six should not be over-interpreted.

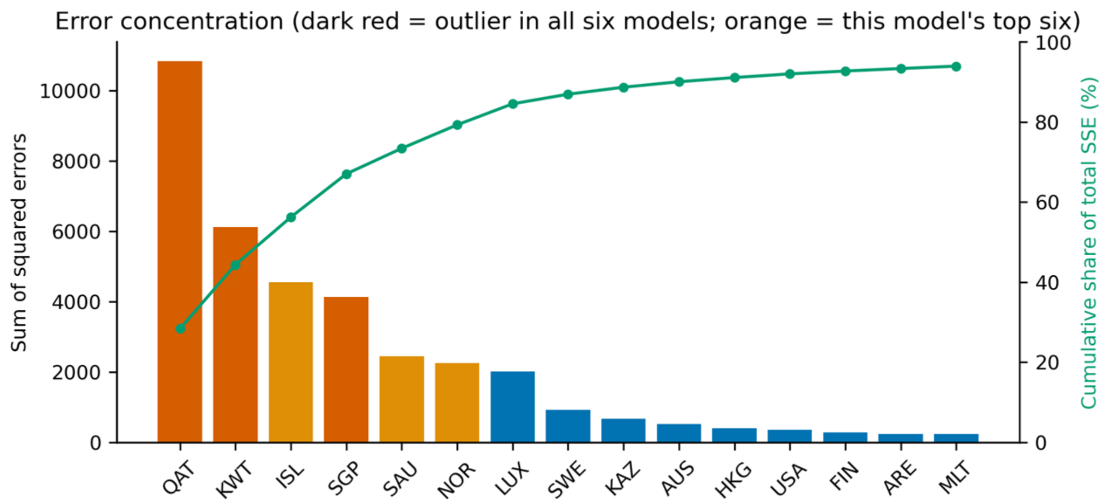

Figure 10. *Pareto decomposition of squared error by country. Dark red marks the three economies that are outliers under every model examined; orange marks the remainder of this model's top six.*

Experiment C tests the implied remedy. Adding the low-carbon share of primary energy on the 76-country sub-panel substantially improves accuracy (Table 4; Figure 11 shows the like-for-like comparison on identical countries). On those same 76 countries, ridge improves from MAPE 22.2% / MdAPE 14.3% to 14.1% / 7.7%, and the ensemble from 21.9% / 13.7% to 14.5% / 7.35%. Median error is therefore roughly halved (−46% for ridge, −46% for the ensemble) while mean error falls by about a third (−36% and −34%). The ensemble is statistically indistinguishable from ridge on this panel ($p = 0.56$) but significantly better than the hybrid alone ($p = 0.0014$), and the hybrid significantly beats LightGBM ($p = 0.0001$). The practical reading is direct: where energy-mix statistics exist, a single covariate is worth more than any architectural innovation evaluated here.

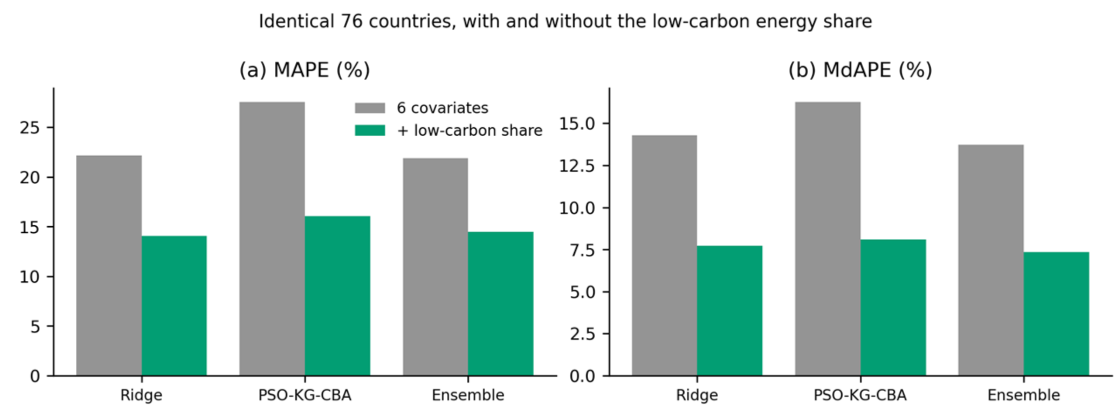

Figure 11. *Effect of adding the low-carbon energy share (identical 76 countries).*

Table 3. Imputation audit for the 112-country panel (3,808 country-years). "Longest run" is the maximum number of consecutive filled years for any single country.

Variable	Filled country-years	% of panel	Longest run (yr)
Per-capita CO_2 (target)	0	0.00	0
Population	0	0.00	0
Oil share	0	0.00	0
Energy per capita	28	0.74	16
GDP per capita	114	2.99	—
Coal share	244	6.41	26
Gas share	291	7.64	31
Low-carbon share (76-country sub-panel)	0	0.00	0

Countries with at least one filled run exceeding three years: 25 of 112. Exceeding ten years: 19 of 112.

Table 4. Out-of-fold LOCO performance, Experiment C (76 countries, 7 covariates).

Model	RMSE	MAE	MAPE (%)	MdAPE (%)	R^2
LightGBM	4.520	2.048	22.8	13.1	0.622
E-PSO-KG-CBA (ours)	3.682	1.593	16.0	8.1	0.749
Ridge	**3.037**	**1.284**	**14.1**	7.7	**0.829**
Ensemble (Ridge + E-PSO-KG-CBA)	3.306	1.409	14.5	**7.35**	0.798

4.4 Regional performance and African case studies

Table 5 gives the full continental breakdown, which is more nuanced than a two-region comparison suggests. On median APE, Europe is easiest (12.5%) and North America hardest (19.6%); Africa (16.8%) sits between Oceania (18.8%) and Asia (15.8%). On *mean* APE the ordering nearly reverses and Africa (26.6%) is close to Europe (23.6%). Africa is therefore not uniformly the hardest region; rather, its error distribution has a heavier right tail, consistent with a small number of countries whose energy structure is poorly proxied.

Table 5. Ensemble absolute percentage error by continent, Experiment A.

Continent	Median APE (%)	Mean APE (%)	75th pct (%)	n (country-years)
Europe	12.50	23.60	25.67	1053
South America	14.84	20.45	26.24	216
Asia	15.83	23.43	26.93	999
Africa	16.77	26.63	26.77	459
Oceania	18.76	18.03	25.22	54

Continent	Median APE (%)	Mean APE (%)	75th pct (%)	n (country-years)
North America	19.63	21.46	27.41	243

Among African economies with fully observed covariate series, leave-country-out accuracy is strong: South Africa attains a median APE of 3.4% and Egypt 5.5% (both with no imputed country-years), and Nigeria 8.0%. Figure 12 shows observed trajectories tracked within the 90% conformal bands of a model that never saw these countries during training. For inventory gap-filling in data-sparse settings, this is the deployment-relevant accuracy level.

Ghana's leave-country-out median APE is 7.4%, but this figure must be read with care and we do not offer it as the study's headline African result: Ghana carries a 26-year filled run in its fuel-share covariates, so its apparently smooth covariate trajectory is substantially an artefact of the edge-extension rule rather than a measured series. The same caveat applies to Cameroon (6.1%, 26 filled years), Rwanda (40.8%, 25 years), Benin (28.0%, 24 years) and Niger (44.8%, 29 years). Restricting the LOCO benchmark to the 87 countries with no filled run longer than three years degrades ridge from MdAPE 16.3% to 17.6% and MAPE 25.2% to 27.5%, confirming that heavily filled countries are *easier* than average and that the full-panel numbers are mildly optimistic. Ghana is thus better read as an illustration of the data-scarcity problem this paper is about than as a demonstration of accuracy under it.

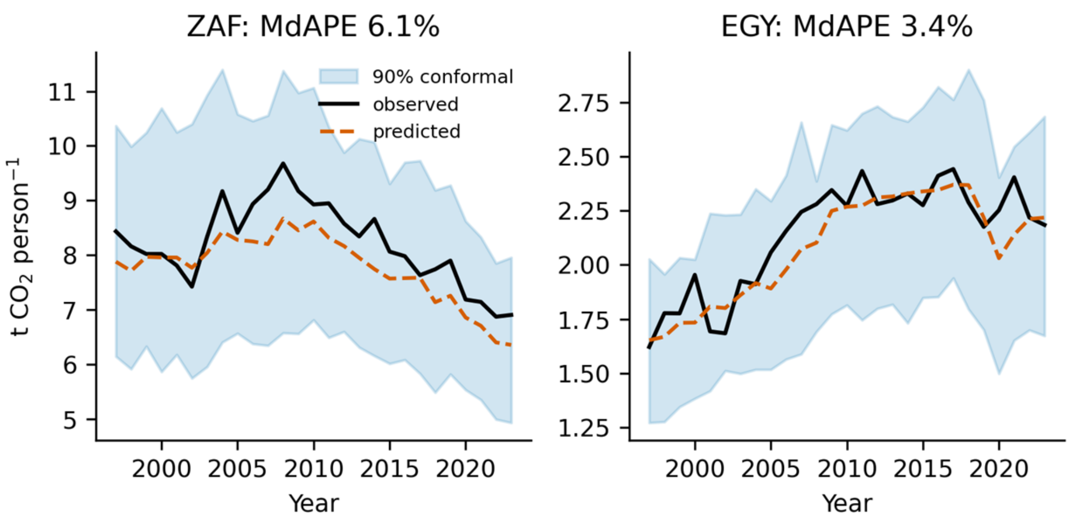

Figure 12. *African case studies with 90% split-conformal intervals. Countries carrying long imputed runs are flagged in the panel titles.*

4.5 Uncertainty calibration

Raw MC-dropout intervals are severely over-confident: at a nominal 90% level they cover only 13.2% of observations with a mean width of 0.47 t person^{-1}. Per-fold split-conformal calibration widens them to an empirical coverage (PICP) of 81.9% with mean interval width 5.68 t person^{-1}. The residual shortfall is attributable to non-exchangeability: calibration and test units belong to disjoint country groups, and fold-level conformal quantiles vary by nearly an order of magnitude (8.8 to 69.2), reflecting heterogeneous country difficulty. This is an honest limitation of split-conformal inference under grouped sampling [35,48], and Section 5.3 outlines group-aware alternatives.

4.6 Explainability

SHAP attributions on the enriched panel (Figure 13) are dominated by log energy per capita (mean |SHAP| = 0.114), an order of magnitude above the low-carbon share (0.016), gas share

(0.008), log population (0.007) and the remaining covariates. Lag-wise attribution decays sharply and monotonically from the most recent window position (t: 0.118; t−1: 0.027; all earlier lags below 0.008), indicating that for this annual-resolution task the contemporaneous covariate vector carries almost all of the tree ensemble's signal and the eight-year window adds little. Both findings are exactly what the Kaya structure of equation (5) predicts, since per-capita energy is the identity's leading term.

This is worth stating plainly because it does *not* corroborate the covariate-availability argument of Section 5.2 in the way one might expect: SHAP ranks the low-carbon share well below energy per capita even though adding that covariate halves median error. The two results are compatible — SHAP measures a feature's contribution to predictions within a fitted model, whereas Experiment C measures the change in generalization error from making the feature available at all, and a covariate can be decisive for the hardest countries while contributing modestly on average. The Experiment C contrast, not the SHAP ranking, is the evidence for the policy argument.

The hybrid's attention weights (Figure 14) range from 0.095 to 0.142 against a uniform 0.125, declining gently from earlier to more recent window positions. Attention is therefore close to uniform pooling, and its value in this architecture lies more in adaptive aggregation than in sharp temporal selection.

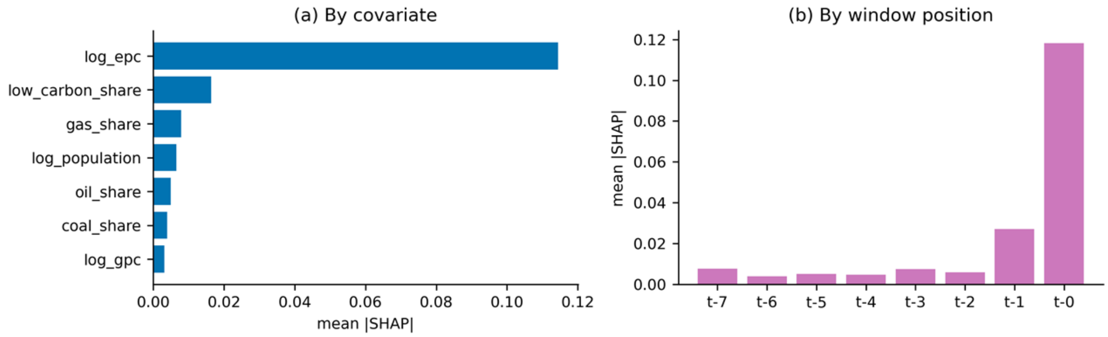

Figure 13. *SHAP attributions on the enriched panel, by covariate and by window position.*

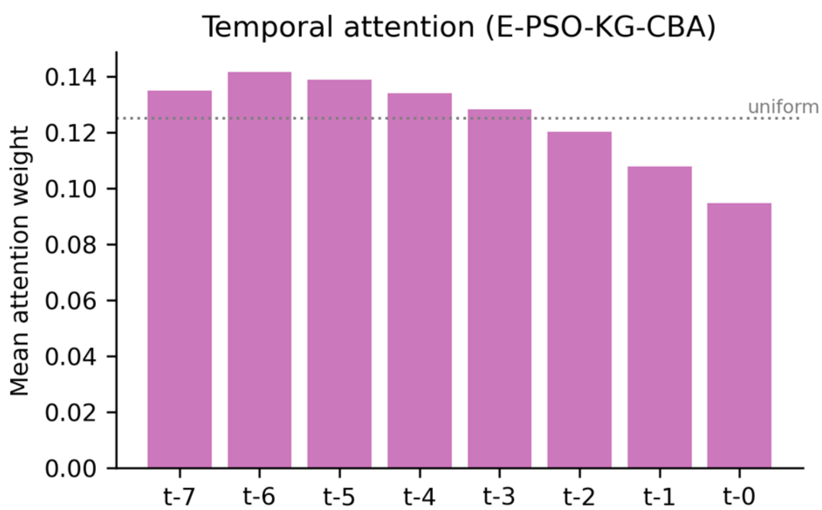

Figure 14. *Mean temporal attention weights by window position. (Supplementary)*

4.7 Experiment B: the persistence benchmark in temporal forecasting

When the same data are recast as conventional forecasting with the target country's own history available, naive persistence proves a formidable benchmark, but not an insurmountable one (Table 6, Figure 15).

At one-year horizons in the 2021-2023 window, persistence attains MAE 0.317 t person^{-1}; only XGBoost improves on it, and by a small and marginally significant margin (level formulation MAE 0.296, $\Delta = -0.021$, cluster-bootstrap $p = 0.045$). Every other learner ties or loses. At three and five years, more learners edge ahead: random forest in log-growth form reaches MAE 0.481 at h = 3 ($p = 0.031$) and 0.621 at h = 5 ($p = 0.039$), and XGBoost 0.599 at h = 5 ($p = 0.0001$). Several learners attain MASE below unity at the longer horizons, with ridge in log-growth form reaching 0.867 at h = 5.

Two qualifications matter more than these point gains. First, the margins are small: the best improvement over persistence at any horizon is 19% of MAE, against a drift baseline that is *worse* than persistence at every horizon in both windows. Second, and decisively, the ranking does not replicate. In the pre-pandemic 2015-2019 window, no learner significantly beats persistence at h = 1 or h = 3, and only random-forest log-growth does so at h = 5 ($p = 0.047$); ridge log-growth attains MASE 0.945 at h = 1 but its advantage is not significant under clustering. The learner that wins in one window is generally not the learner that wins in the other.

The implication for the literature is therefore narrower than a blanket claim that learning fails, but no less pointed. Annual national per-capita CO_2 is close enough to a random walk that persistence must always be reported; margins over it are of order 5-15% of MAE, are horizon-dependent, and are not stable across evaluation periods. Reported temporal R^2 values near unity, published without a naive baseline, largely re-describe persistence rather than demonstrate skill. The log-growth target formulation matters more than the choice of learner. The LOCO formulation is immune to this artefact because the target country's history is withheld by construction.

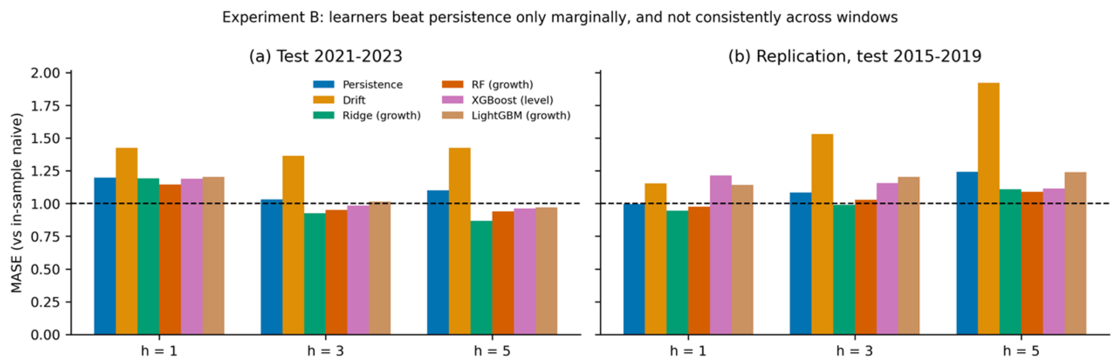

Figure 15. *Experiment B: MASE against the in-sample naive benchmark, both evaluation windows. Values below the dashed line indicate skill.*

Table 6. Experiment B, MAE (t CO_2 person^{-1}) and MASE by horizon. Bold marks a significant improvement over persistence under a country cluster bootstrap ($p < 0.05$).

Model	h=1 MAE	h=3 MAE	h=5 MAE	h=1 MASE	h=3 MASE	h=5 MASE
Test window 2021-2023						
Persistence	0.317	0.531	0.738	1.198	1.030	1.101
Drift	0.380	0.680	0.933	1.425	1.363	1.424
Ridge (log-growth)	0.339	0.542	0.678	1.193	0.926	0.867
Random forest (log-growth)	0.307	**0.481**	**0.621**	1.145	0.950	0.939
XGBoost (level)	**0.296**	0.506	**0.599**	1.188	0.983	0.963
LightGBM (log-growth)	0.307	0.528	0.621	1.202	1.014	0.971
Replication window						

Model	h=1 MAE	h=3 MAE	h=5 MAE	h=1 MASE	h=3 MASE	h=5 MASE
2015-2019						
Persistence	0.247	0.468	0.682	0.995	1.084	1.241
Drift	0.285	0.683	1.043	1.154	1.531	1.920
Ridge (log-growth)	0.239	0.429	0.598	0.945	0.990	1.108
Random forest (log-growth)	0.246	0.453	**0.567**	0.976	1.028	1.088
XGBoost (level)	0.302	0.457	0.642	1.213	1.155	1.114
LightGBM (log-growth)	0.269	0.516	0.647	1.141	1.204	1.238

5. Discussion

5.1 Why physics guidance matters more than depth

The central empirical message is structural. In log space, the Kaya identity makes cross-country emission variation approximately linear in energy and fuel-mix covariates; unguided deep networks spend most of their capacity rediscovering this plane from roughly 2,400 training samples and still fall significantly short of ridge regression. Encoding the plane explicitly, warm-starting a linear head at the ridge solution and letting the deep branch model only residuals, recovers the deep models' competitiveness: both Kaya-guided hybrids significantly outperform the identical unguided architecture on median error. Yet the hybrids' remaining weakness is instructive: their R^2 lags ridge badly (0.55 versus 0.80) because residual capacity occasionally amplifies errors on extreme-scale economies, so they win on the median and lose on the mean square.

Ensembling narrows this asymmetry but, on the evidence of clustered inference, does not beat ridge alone. That negative result is the honest one, and it sharpens rather than weakens the paper's message. For applied emission modelling the ordering of returns is: correct covariates first, physics-informed structure second, ensembling third, architectural novelty last. A study that had tested at the observation level would have reported the ensemble as decisively best ($p < 10^{-9}$) and drawn the opposite methodological lesson.

5.2 Policy implications for inventory gap-filling

Experiment C converts a modelling observation into a statistical-capacity argument. One additional covariate, the low-carbon share of primary energy, halves leave-country-out median error and collapses the outlier problem, because it measures exactly the carbon-intensity term that fossil-fuel shares cannot see. Most African economies lack this statistic in the international energy lineages.

The imputation audit sharpens the same point from an unexpected direction. Of the 25 panel countries carrying filled runs longer than three years, the overwhelming majority are low- and middle-income, and nine are African. These are countries for which the international energy statistics are so thin that a balanced panel can only be constructed by carrying a single observation across two or three decades. Ghana is a case in point: it enters this study's panel only because 26 years of its fuel-share series are extended from a handful of observations. The binding constraint on emission transparency in these countries is therefore not model capacity and not even the low-carbon covariate specifically, but the absence of basic, annually updated national energy balances. Investment there would yield disproportionate returns for Enhanced Transparency Framework implementation in non-Annex I countries [3-6,43], plausibly more than further model development. Where such balances do exist, as for South Africa and Egypt, leave-country-out estimation already achieves 3-6% median error without the country ever being observed.

5.3 Limitations and threats to validity

Six limitations qualify the findings. First, the balanced-panel requirement retains 112 countries, and 25 of these are retained only through long constant extension of their covariate series; the sensitivity analysis of Section 4.4 shows the full-panel results are mildly optimistic as a consequence, and the states most in need of gap-filling remain under-represented even so. Second, the three fuel-share covariates are ratios derived from CO_2 accounts rather than energy balances. They carry no information about the emission *level*, but a country with no inventory at all would not have them. The ablation in Section 4.2 bounds this concern tightly: removing them raises MdAPE by only 0.6 percentage points, so the reported accuracy is not an artefact of emission-account provenance. Third, conformal coverage falls eight points short of nominal under grouped sampling; group-conditional conformal methods and non-exchangeability-robust weightings [35,48] are the natural remedies. Fourth, PSO was run with a modest budget (30 evaluations) on a single fold's inner split; larger budgets or multi-fold fitness could improve the hybrid further. Fifth, the ensemble composition was selected after inspecting out-of-fold results, which is one reason we do not claim significance for its margin over ridge. Finally, our Experiment B conclusions concern annual national aggregates over one- to five-year horizons and do not preclude learnable structure at finer temporal or spatial resolutions.

6. Conclusions

This study reframed national CO_2 modelling around the question inventories actually pose, estimating emissions for countries without usable emission records, and benchmarked thirteen models under strictly country-disjoint validation with country-clustered inference throughout. A physics-guided hybrid, KG-CBA, tuned by particle swarm optimization, significantly improves the identical unguided architecture (median APE 15.7-16.7% vs 20.8%), and a Kaya-motivated ridge regression significantly outperforms every tree ensemble and every unguided deep network. The best ensemble attains the study's lowest point error (MAPE 23.5%, MdAPE 15.1% across 112 countries; MdAPE 7.35% with enriched covariates on 76 countries) but its advantage over ridge alone is not statistically significant once repeated years within countries are accounted for — a distinction that observation-level testing would have concealed.

Error analysis identified energy-mix data availability as the binding constraint, quantified the cost of its absence, and located it geographically in the countries least able to report. Where national energy balances exist, leave-country-out estimation reaches 3-6% median error for African economies such as South Africa and Egypt; where they do not, panels can be assembled only by extending sparse observations across decades, which is itself the clearest statement of the problem.

Equally important are the study's negative results: unguided deep architectures do not beat a Kaya-motivated linear model in this regime; ensembling does not significantly beat that linear model either; split-conformal intervals under-cover under grouped sampling; SHAP does not rank the decisive covariate first; and in conventional temporal forecasting, learners beat naive persistence only by small margins that fail to replicate across evaluation windows. Future work will extend the framework to sectoral and subnational estimation, group-aware conformal calibration, and transfer to the full set of reporting-gap countries as covariate coverage improves.

Funding

This research received no specific grant from any funding agency in the public, commercial, or not-for-profit sectors.

Ethics statement

This study used only publicly available, country-level aggregate statistics. It involved no human participants, no animal subjects, and no personal or identifiable data, so no ethics approval was required.

Acknowledgements

The authors thank the Global Carbon Project, the Energy Institute, and Our World in Data for maintaining and openly publishing the datasets on which this work depends.

CRediT authorship contribution statement

S.C. Atuahene: Conceptualization, Methodology, Software, Formal analysis, Investigation, Data curation, Visualization, Writing - original draft. **B. Boateng:** Supervision, Resources, Writing - review & editing. **H. Amarfio:** Investigation, Validation, Writing - review & editing. **E. Y. Quayson:** Investigation, Validation, Writing - review & editing. **F.B. Agyenim:** Investigation, Validation, Writing - review & editing.

Declaration of competing interest

The authors declare no competing financial interests or personal relationships that could have influenced this work.

Data and code availability

All data are openly available: Our World in Data CO_2 and energy datasets (https://github.com/owid/co2-data; https://github.com/owid/energy-data), redistributing the Global Carbon Budget and the Energy Institute Statistical Review of World Energy. The complete analysis pipeline, harmonized panel, per-fold out-of-fold prediction vectors for every model, and the fold-level model checkpoints for the enriched hybrid are openly available at https://github.com/samfozzy/kg-cba-loco-co2-reproducibility. This repository contains the harmonized panel, the complete analysis pipeline (build_panel.py, which regenerates the panel exactly from the raw downloads; classical and deep LOCO baselines, PSO tuning, enriched-panel models, conformal calibration, explainability, Experiment B, and the clustered significance analysis), per-fold out-of-fold prediction vectors for every model, the fold-level model checkpoints for the enriched hybrid, and all scripts that generate the figures and tables in this paper. REPRODUCE.md in that repository documents the run order and expected outputs.

Declaration on the use of generative AI

During the preparation of this work the authors used Claude (Anthropic) to assist with code development for the experimental pipeline, statistical analysis, figure generation, and drafting of the manuscript text. The authors reviewed and edited all content and take full responsibility for the integrity and accuracy of the publication.

ORCID iDs:

Samiuel C. Atuahene: https://orcid.org/0000-0002-2928-6458;

Bismark Boateng: https://orcid.org/0000-0003-3906-5277;

Hilda Amarfio: https://orcid.org/0009-0006-0806-5919;

Ekow Yaleh Quayson: https://orcid.org/0009-0006-3516-3434;

Francis Boateng Agyenim: https://orcid.org/0000-0003-4986-2261;

References

[1] United Nations Environment Programme. Emissions Gap Report 2025: Off Target: Continued Collective Inaction Puts Global Temperature Goal at Risk. UNEP, Nairobi, 2025.

[2] Friedlingstein P, O'Sullivan M, Jones MW, Andrew RM, Hauck J, Landschützer P, Le Quéré C, Li H, Luijkx IT, Olsen A, et al. Global Carbon Budget 2024. Earth System Science Data 2025;17:965-1039.

[3] Dittmer KM, Wollenberg E, Cohen M, Egler C. How good is the data for tracking countries' agricultural greenhouse gas emissions? Making use of multiple national greenhouse gas inventories. Frontiers in Sustainable Food Systems 2023;7:1156822. https://doi.org/10.3389/fsufs.2023.1156822

[4] Mostefaoui M, Ciais P, McGrath MJ, Peylin P, Patra PK, Ernst Y. Greenhouse gas emissions and their trends over the last three decades across Africa. Earth System Science Data 2024;16:245-275. https://doi.org/10.5194/essd-16-245-2024

[5] OECD. National greenhouse gas emission inventories: filling the gaps in official data. OECD Publishing, Paris, 2024. https://doi.org/10.1787/f19f1663-en

[6] Machine learning estimates for G20 subnational urban GHG emissions from 2000-2020. Scientific Data 2026;13. https://doi.org/10.1038/s41597-026-06691-9

[7] Exploring machine learning models for predicting greenhouse gas emissions in Africa's building sector: a case study of six nations. Environmental Systems Research 2025;14. https://doi.org/10.1186/s40068-025-00407-5

[8] Determinants of carbon emissions in Africa: new evidence based on machine learning algorithms. Environment, Development and Sustainability 2024. https://doi.org/10.1007/s10668-024-05566-6

[9] Evaluating the machine learning-based models for predicting carbon neutrality in Sub-Saharan African nations. Environment, Development and Sustainability 2025. https://doi.org/10.1007/s10668-025-06289-y

[10] Predicting transportation-related greenhouse gas emissions in Africa's top emitters: a machine learning approach. Environmental Sciences Europe 2025;37. https://doi.org/10.1186/s12302-025-01223-5

[11] Ajala AA, Adeoye OL, Salami OM, Jimoh AY. An examination of daily CO2 emissions prediction through a comparative analysis of machine learning, deep learning, and statistical models. Environmental Science and Pollution Research 2025. [PMC11802685]

[12] Multivariate CO2 emissions forecasting using deep neural network architectures. Machine Learning and Knowledge Extraction 2026;8(1):12. https://doi.org/10.3390/make8010012

[13] Evaluating deep learning architectures for CO2 emissions forecasting: TCN, LSTM, and hybrid approaches with hyperparameter optimization. Eastern-European Journal of Enterprise Technologies 2025;5(4). https://journals.uran.ua/eejet/article/view/331523

[14] A hybrid CNN-BiLSTM-attention model with feature engineering for accurate carbon emission forecasting. Air Quality, Atmosphere & Health 2026. https://doi.org/10.1007/s11869-026-01954-1

[15] Wang R. Carbon emission prediction for gas power plants based on deep learning under small-sample conditions. Concurrency and Computation: Practice and Experience 2026;38. https://doi.org/10.1002/cpe.70591

[16] Hybrid neural network-based maritime carbon dioxide emission prediction incorporating dynamics for enhanced accuracy. Applied Sciences 2025;15(9):4654. https://doi.org/10.3390/app15094654

[17] Yin C, Wu J, Sun X, Meng Z, Lee C. Road transportation emission prediction and policy formulation: machine learning model analysis. Transportation Research Part D 2024;135:104390. https://doi.org/10.1016/j.trd.2024.104390

[18] Kong F, Song J, Yang Z. A novel short-term carbon emission prediction model based on secondary decomposition method and long short-term memory network. Environmental Science and Pollution Research 2022;29(43):64983-64998. https://doi.org/10.1007/s11356-022-20393-w

[19] Optimised deep learning for time-critical load forecasting using LSTM and modified particle swarm optimisation. Energies 2024;17(22):5524. https://doi.org/10.3390/en17225524

[20] Short-term load forecasting using a particle-swarm optimized multi-head attention-augmented CNN-LSTM network. arXiv preprint 2023;arXiv:2309.03694.

[21] Predicting CO2 emissions with advanced deep learning models and a hybrid Greylag Goose optimization algorithm. Mathematics 2025;13(9):1481. https://doi.org/10.3390/math13091481

[22] Makridakis S, Spiliotis E, Assimakopoulos V. M5 accuracy competition: results, findings, and conclusions. International Journal of Forecasting 2022;38(4):1346-1364. https://doi.org/10.1016/j.ijforecast.2021.11.013

[23] Makridakis S, Spiliotis E, Assimakopoulos V, Chen Z, Gaba A, Tsetlin I, Winkler RL. The M5 uncertainty competition: results, findings and conclusions. International Journal of Forecasting 2022;38(4):1365-1385.

[24] Makridakis S, et al. The M6 forecasting competition: bridging the gap between forecasting and investment decisions. International Journal of Forecasting 2024.

[25] Energy Institute. Statistical Review of World Energy 2024. Energy Institute, London, 2024.

[26] Ritchie H, Rosado P, Roser M. CO2 and greenhouse gas emissions. Our World in Data, 2024. https://ourworldindata.org/co2-and-greenhouse-gas-emissions

[27] Kaya Y. Impact of carbon dioxide emission control on GNP growth: interpretation of proposed scenarios. IPCC Energy and Industry Subgroup, Response Strategies Working Group, Paris, 1990.

[28] Decomposing CO2 emissions with the Kaya identity: global trends, national dynamics, and policy implications. Sustainability 2026;18(3):1627. https://doi.org/10.3390/su18031627

[29] Kennedy J, Eberhart R. Particle swarm optimization. Proceedings of ICNN'95 - International Conference on Neural Networks 1995;4:1942-1948.

[30] Varied drivers for reducing CO2 emissions in countries with legislated carbon neutrality targets: a Kaya identity clustering analysis. Environment, Development and Sustainability 2025. https://doi.org/10.1007/s10668-025-06223-2

[31] Bacanin N, Simic V, Zivkovic M, Alrasheedi M, Petrovic A. Cloud computing load prediction by decomposition reinforced attention long short-term memory network optimized by

modified particle swarm optimization algorithm. Annals of Operations Research 2023. https://doi.org/10.1007/s10479-023-05745-0

[32] Gal Y, Ghahramani Z. Dropout as a Bayesian approximation: representing model uncertainty in deep learning. Proceedings of the 33rd International Conference on Machine Learning (ICML) 2016;48:1050-1059.

[33] Fontana M, Zeni G, Vantini S. Conformal prediction: a unified review of theory and new challenges. Bernoulli 2023;29(1):1-23. https://doi.org/10.3150/21-BEJ1447

[34] Jensen V, Bianchi FM, Anfinsen SN. Ensemble conformalized quantile regression for probabilistic time series forecasting. IEEE Transactions on Neural Networks and Learning Systems 2024;35(7):9014-9025. https://doi.org/10.1109/TNNLS.2022.3217694

[35] Barber RF, Candès EJ, Ramdas A, Tibshirani RJ. Conformal prediction beyond exchangeability. Annals of Statistics 2023;51(2):816-845. https://doi.org/10.1214/23-AOS2276

[36] Lundberg SM, Lee S-I. A unified approach to interpreting model predictions. Advances in Neural Information Processing Systems 2017;30:4765-4774.

[37] Ağbulut Ü. Forecasting of transportation-related energy demand and CO2 emissions in Turkey with different machine learning algorithms. Sustainable Production and Consumption 2022;29:141-157. https://doi.org/10.1016/j.spc.2021.10.001

[38] Janhuaton T, Ratanavaraha V, Jomnonkwao S. Forecasting Thailand's transportation CO2 emissions: a comparison among artificial intelligent models. Forecasting 2024;6(2):462-484. https://doi.org/10.3390/forecast6020026

[39] Li S, Tong Z, Haroon M. Estimation of transport CO2 emissions using machine learning algorithm. Transportation Research Part D 2024;133:104276. https://doi.org/10.1016/j.trd.2024.104276

[40] Jha R, Jha R, Islam M. Forecasting US data center CO2 emissions using AI models: emissions reduction strategies and policy recommendations. Frontiers in Sustainability 2025;5:1507030. https://doi.org/10.3389/frsus.2024.1507030

[41] Tian L, Zhang Z, He Z, Yuan C, Xie Y, Zhang K, Jing R. Predicting energy-based CO2 emissions in the United States using machine learning: a path toward mitigating climate change. Sustainability 2025;17(7):2843. https://doi.org/10.3390/su17072843

[42] A framework for carbon footprint computation and forecasting for Nigeria's industrial decarbonization plan (NIDP). Frontiers in Energy Research 2026;13:1717733. https://doi.org/10.3389/fenrg.2026.1717733

[43] Kaya identity-based decomposition and machine-learning perspectives on US energy-related CO2 emissions 2024. U.S. Energy Information Administration, Washington DC, 2025.

[44] LSTM hyperparameter tuning via modified metaheuristics: an application in renewable energy forecasting. In: Lecture Notes in Networks and Systems. Springer, Cham, 2025. https://doi.org/10.1007/978-3-031-98304-7_74

[45] Vovk V, Gammerman A, Shafer G. Algorithmic Learning in a Random World. Springer, New York, 2005.

[46] Comparative analysis of conformal prediction techniques and machine learning models for very short-term solar power forecasting. Energy and AI 2025. https://doi.org/10.1016/j.egyai.2025.100513

[47] Renkema Y, Visser L, AlSkaif T. Enhancing the reliability of probabilistic PV power forecasts using conformal prediction. Solar Energy Advances 2024;4:100059. https://doi.org/10.1016/j.seja.2024.100059

[48] Oliveira RI, Orenstein P, Ramos T, Romano JV. Split conformal prediction and non-exchangeable data. Journal of Machine Learning Research 2024;25(225):1-38.

[49] An interpretable machine learning-based framework for CO2 emission prediction and optimization: a case study of a university campus. Sustainability 2025;17(23):10432. https://doi.org/10.3390/su172310432

[50] Deep learning model based prediction of vehicle CO2 emissions with explainable AI integration for sustainable environment. Scientific Reports 2025;15. https://doi.org/10.1038/s41598-025-87233-y

[51] A multi-stage feature selection and explainable machine learning framework for forecasting transportation CO2 emissions. Energies 2025;18(15):4184. https://doi.org/10.3390/en18154184

[52] Chen T, Guestrin C. XGBoost: a scalable tree boosting system. Proceedings of the 22nd ACM SIGKDD International Conference on Knowledge Discovery and Data Mining 2016:785-794.

[53] Ke G, Meng Q, Finley T, Wang T, Chen W, Ma W, Ye Q, Liu T-Y. LightGBM: a highly efficient gradient boosting decision tree. Advances in Neural Information Processing Systems 2017;30:3146-3154.

[54] Hochreiter S, Schmidhuber J. Long short-term memory. Neural Computation 1997;9(8):1735-1780.

[55] Bahdanau D, Cho K, Bengio Y. Neural machine translation by jointly learning to align and translate. International Conference on Learning Representations (ICLR) 2015.

Nomenclature

Symbol	Description	Symbol	Description
$c_{i,t}$	Per-capita CO_2 (t $person^{-1}$ yr^{-1})	α_τ	Attention weight at window step τ
$y_{i,t}$	$\ln c_{i,t}$, modelling target	$\mathbf{s}$	Attention context vector
E,G,P	Energy, GDP, population	$\boldsymbol{\beta}$	Kaya-head (ridge) coefficients
s^{coal},s^{oil},s^{gas}	Fuel shares of CO_2	$r_{\boldsymbol{\theta}}$	Deep residual branch
s^{lc}	Low-carbon share of primary energy	ω,c_1,c_2	PSO inertia, cognitive, social constants
$\mathbf{X}_{i,t}$	8-year covariate window (W × F)	$\mathbf{p}_j$,$\mathbf{v}_j$	PSO particle position, velocity
W,F	Window length (8), feature count (6/7)	T	MC-dropout forward passes (60)
$\boldsymbol{\mu}_{tr}$,$\boldsymbol{\sigma}_{tr}$	Fold-wise standardization	$\hat{q}$	Conformal quantile

Symbol	Description	Symbol	Description
	moments		
f,**i**,**o**	LSTM forget/input/output gates	s_n	Normalized nonconformity score
z,**r**	GRU update/reset gates	ϕ_j	SHAP value of feature j
$\mathbf{h}_\tau$	Hidden state at step τ	MASE_h	Mean absolute scaled error, horizon h
$\mathbf{K}^{(l)}$	Conv1D kernel, layer l	PICP/MPIW	Interval coverage / mean width

Appendix A. Algorithms

Algorithm A1: PSO hyperparameter optimization of KG-CBA.

```
Input: bounds [l,u] for (filters, kernel, units, dropout, log-lr, batch);
    swarm size J=6, iterations K=5; country-disjoint train/val split of fold 1
Initialize positions p_j ~ U(l,u), velocities v_j ~ U(-1,1)·0.15(u-l)
for k = 1..K:
  for j = 1..J:
    hp <- decode(p_j)                # round ints, exponentiate lr
    model <- build_KG_CBA(hp); warm-start Kaya head at last-step ridge solution
    train with early stopping (patience 6, <=60 epochs) on inner val
    f_j <- min validation MSE; checkpoint state to disk
    update personal best (p_j*, f_j*) and global best (g*, f*)
  v_j <- 0.7 v_j + 1.5 r1 (p_j* - p_j) + 1.5 r2 (g* - p_j);  clip to 0.3(u-l)
```

```
  p_j <- clip(p_j + v_j, l, u)
Output: g* = (37, 4, 40, 0.231, 9.96e-4, 48), f* = 0.0522
```

Algorithm A2: KG-CBA training with ridge warm start (per fold).

```
Input: fold-k training countries; inner split by country (6/7 train, 1/7 val)
1. Standardize windows with training moments (mu_tr, sigma_tr)
2. Fit ridge (lambda=1) on LAST-STEP covariates -> (beta, beta0)
3. Build network: Dense(1) Kaya head initialized at (beta, beta0);
   Conv1D x2 -> BiLSTM -> dropout -> additive attention -> Dense(32) ->
   residual head initialized ~ N(0, 1e-3); output = Kaya head + residual
4. Train jointly, Adam(lr), MSE loss, early stopping patience 9, <=90 epochs
5. Save model and scaler; predict held-out countries of fold k
```

Algorithm A3: Country-clustered comparison of two models.

```
Input: out-of-fold APE vectors a, b over N country-years; country labels g
1. p_obs     <- Wilcoxon signed-rank(a, b)             # reported for contrast only
2. per-country medians A_c = median(a | g=c), B_c likewise
   p_country  <- Wilcoxon signed-rank(A, B) over the C countries
3. cluster bootstrap: for r = 1..10000
       draw C country labels with replacement
       delta_r <- median(pooled a - b over drawn countries)
   CI  <- 2.5th and 97.5th percentiles of delta
   p_boot <- 2 * min(P(delta<=0), P(delta>=0))
Output: (p_obs, p_country, delta, CI, p_boot); conclude from p_boot
```

Appendix B. Extended tables

Table B1. PSO search space and converged configuration.

Hyperparameter	Range	Best
Conv1D filters	[16, 64]	37
Kernel size	{2, 3, 4}	4
BiLSTM units	[16, 96]	40
Dropout	[0.05, 0.45]	0.231
Learning rate	[2×10^{-4}, 3×10^{-3}] (log)	9.96×10^{-4}
Batch size	{48, 64, 96, 128}	48

Table B2. Per-fold MdAPE (%) of the leading models, Experiment A. Fold heterogeneity motivates the block-level uncertainty treatment.

Fold	Ridge	GRU	PSO-KG-CBA	Ensemble
1	11.6	15.7	11.7	10.1
2	23.2	29.5	24.9	25.6
3	18.1	18.4	17.7	18.3
4	15.8	14.2	17.6	13.7
5	13.8	17.3	13.0	10.7

Table B6. Covariate ablation, ridge regression under identical LOCO folds.

Covariate set	RMSE	MAE	MAPE (%)	MdAPE (%)	R^2
All six (energy, GDP, population, three fuel shares)	3.056	1.443	25.2	16.3	0.800
Energy, GDP, population only (no CO_2-derived inputs)	3.244	1.567	26.7	16.9	0.775
Log energy per capita only	3.595	1.690	28.5	17.9	0.723

858 **Table B3.** Positioning against representative prior studies of ML-based CO_2 modelling.

Study	Task	Country-disjoint CV	Naive baseline	Clustered inference	Physics guidance	UQ
Ajala et al. 2025 [11]	Daily forecasting, 4 regions	No	Partial	No	No	No
MAKE 2026 [12]	Multivariate forecasting	No	No	No	No	No
AQAH 2026 [14]	Daily national forecasting	No	No	No	No	No
CCPE 2026 [15]	Plant-level prediction	No	No	No	No	No

Study	Task	Country-disjoint CV	Naive baseline	Clustered inference	Physics guidance	UQ
Applied Sciences 2025 [16]	Maritime emissions	No	No	No	No	No
Africa studies [7-10]	Sectoral prediction	No	No	No	No	No
Sci. Data 2026 [6]	Subnational gap-filling	Partial	No	No	No	Partial
This study	**LOCO inventory-gap estimation**	**Yes (grouped 5-fold)**	**Yes (persistence, drift, MASE)**	**Yes (cluster bootstrap)**	**Yes (Kaya head)**	**Yes (conformal MC-dropout)**

Columns record whether each study's *published* protocol includes the listed safeguard, as reported in its methods section; a "No" indicates the safeguard is not described rather than that it was tested and omitted.

Table B4. The 112 economies of the main panel: AFG, ALB, ARE, ARG, ARM, AUS, AUT, AZE, BEL, BEN, BGD, BGR, BIH, BLR, BOL, BRA, BWA, CAN, CHE, CHL, CHN, CMR, COD, COL, CUB, CYP, CZE, DEU, DNK, DOM, DZA, EGY, ESP, EST, FIN, FRA, GBR, GEO, GHA, GRC, GTM, HKG, HRV, HUN, IDN, IND, IRL, IRN, IRQ, ISL, ISR, ITA, JAM,

JOR, JPN, KAZ, KGZ, KOR, KWT, LBN, LBY, LTU, LUX, LVA, MAR, MDA, MEX, MKD, MLT, MMR, MOZ, MYS, NER, NGA, NLD, NOR, NZL, OMN, PAK, PAN, PER, PHL, POL, PRT, QAT, ROU, RUS, RWA, SAU, SEN, SGP, SLV, SRB, SVK, SVN, SWE, SYR, THA, TJK, TKM, TUN, TUR, TWN, TZA, UKR, URY, USA, UZB, VEN, VNM, YEM, ZAF. The 76-country enriched sub-panel comprises those with ≥90% low-carbon-share coverage. Per-country imputation status is given in table_imputation_runs.csv.

Table B5. Countries with the longest filled covariate runs (top 12 of the 25 exceeding three years).

ISO	Longest filled run (yr)	ISO	Longest filled run (yr)
SLV	31	RWA	25
NER	29	BEN	24
PAN	28	BOL	21
GHA	26	LBY	15
JAM	26	SEN	12
GTM	26	TUN	11
CMR	26	TZA	9

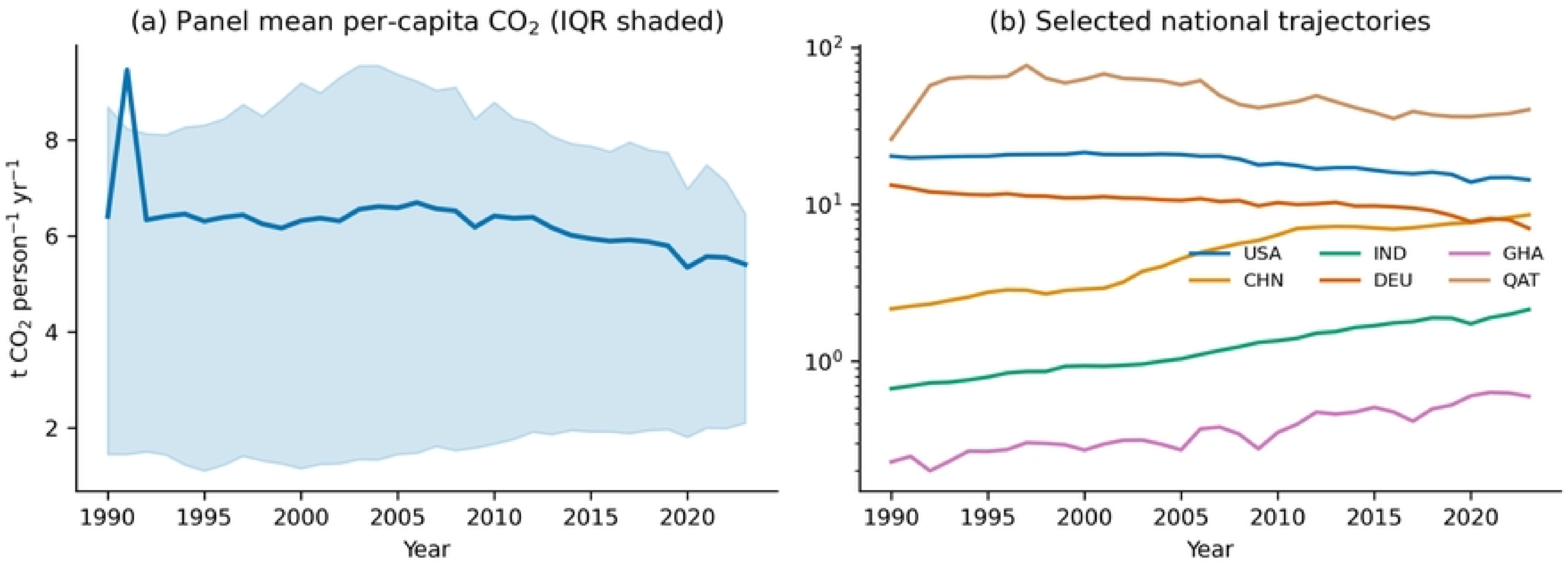

(a) Panel mean per-capita CO_2 (IQR shaded)
t CO_2 person^{-1} yr^{-1}
8
6
4
2
1990
1995
2000
2005
2010
2015
2020
Year
(b) Selected national trajectories
10^2
10^1
10^0
USA
CHN
IND
DEU
GHA
QAT
1990
1995
2000
2005
2010
2015
2020
Year

F01

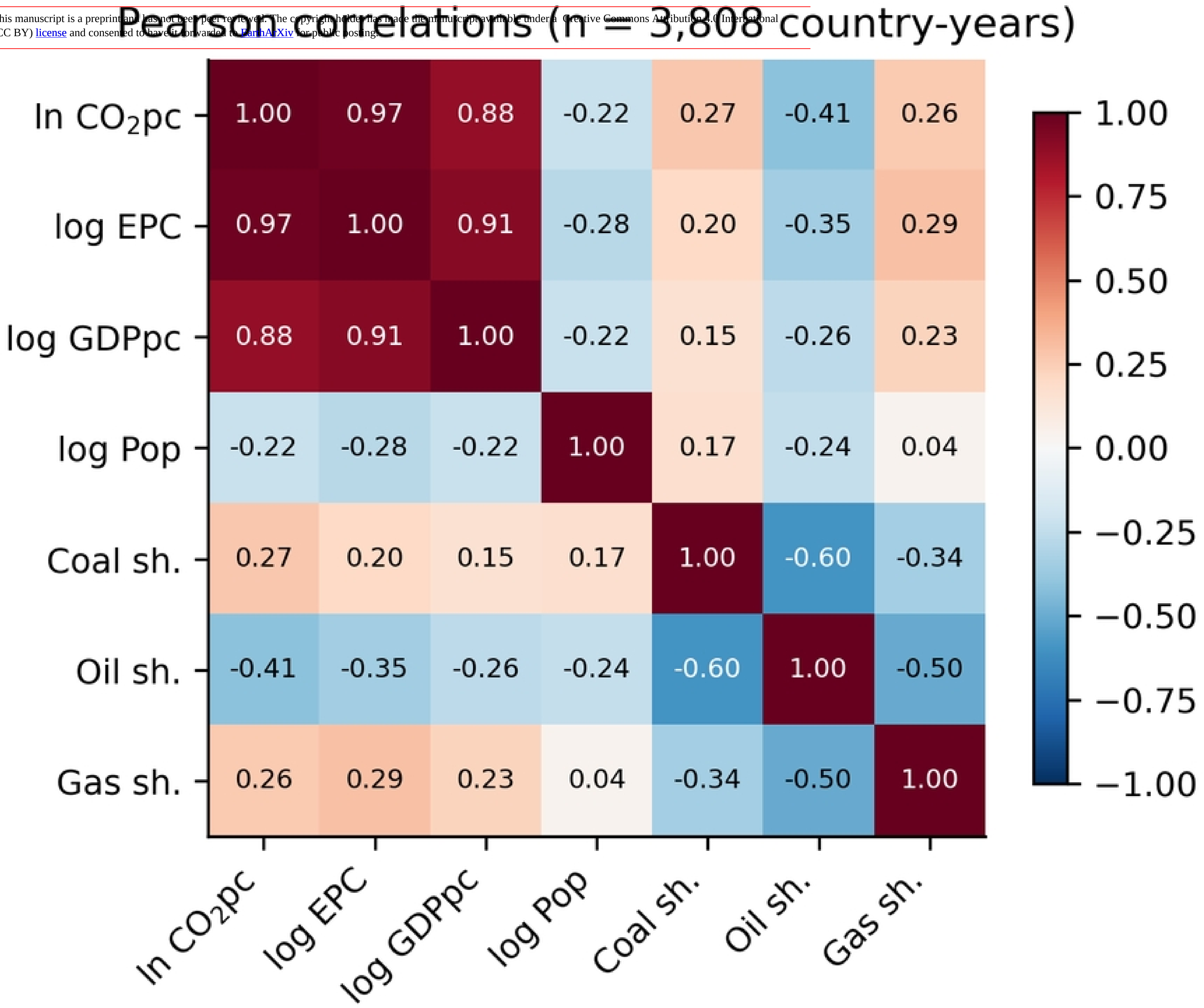
Pearson correlations (n = 3,808 country-years)
ln CO2pc
log EPC
log GDPpc
log Pop
Coal sh.
Oil sh.
Gas sh.
1.00 0.97 0.88 -0.22 0.27 -0.41 0.26
0.97 1.00 0.91 -0.28 0.20 -0.35 0.29
0.88 0.91 1.00 -0.22 0.15 -0.26 0.23
-0.22 -0.28 -0.22 1.00 0.17 -0.24 0.04
0.27 0.20 0.15 0.17 1.00 -0.60 -0.34
-0.41 -0.35 -0.26 -0.24 -0.60 1.00 -0.50
0.26 0.29 0.23 0.04 -0.34 -0.50 1.00
1.00
0.75
0.50
0.25
0.00
−0.25
−0.50
−0.75
−1.00

F02

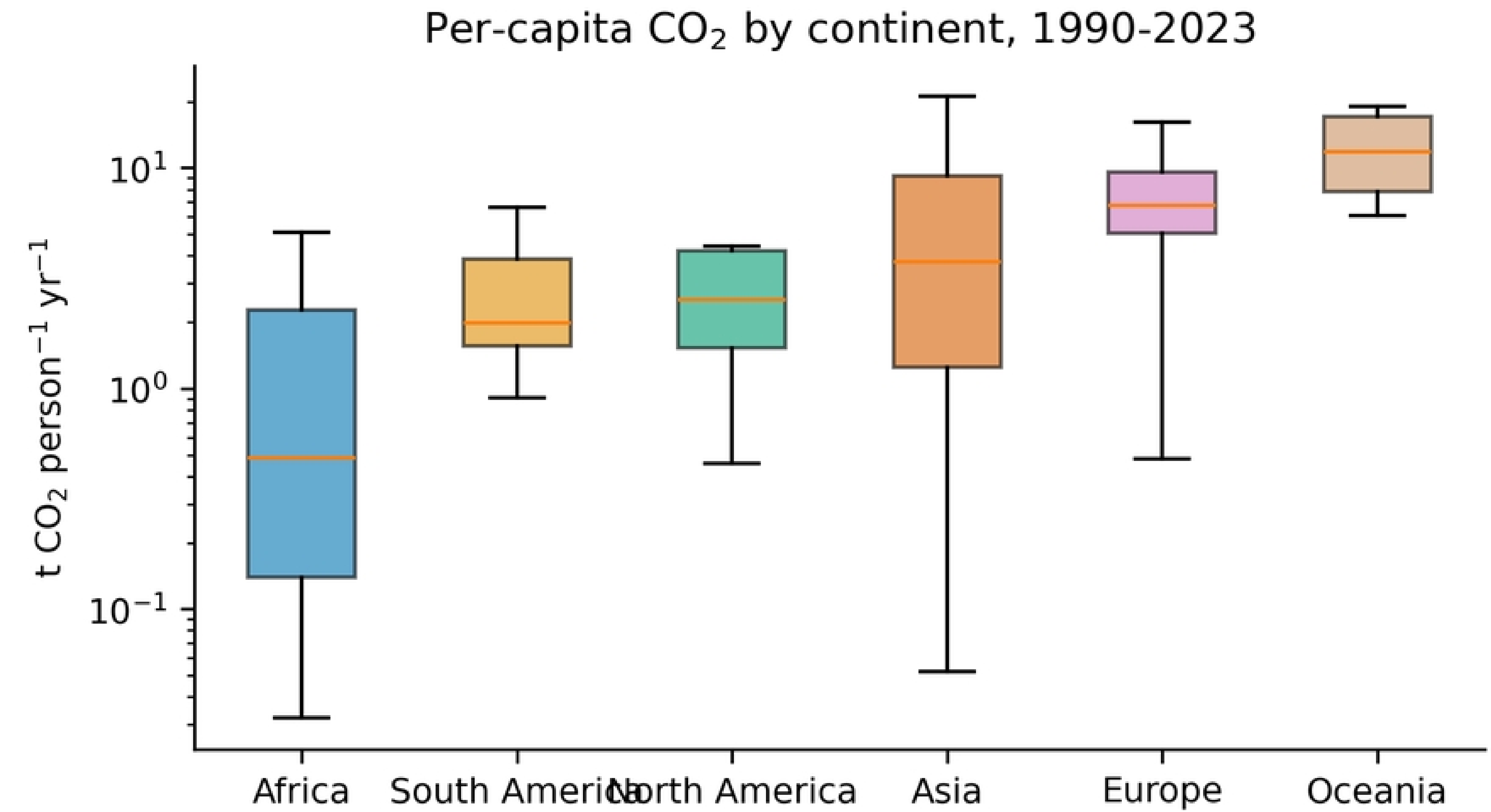

Per-capita CO_2 by continent, 1990-2023
t CO_2 person^{-1} yr^{-1}
10^1
10^0
10^{-1}
Africa
South America
North America
Asia
Europe
Oceania

F03

Experimental framework overview

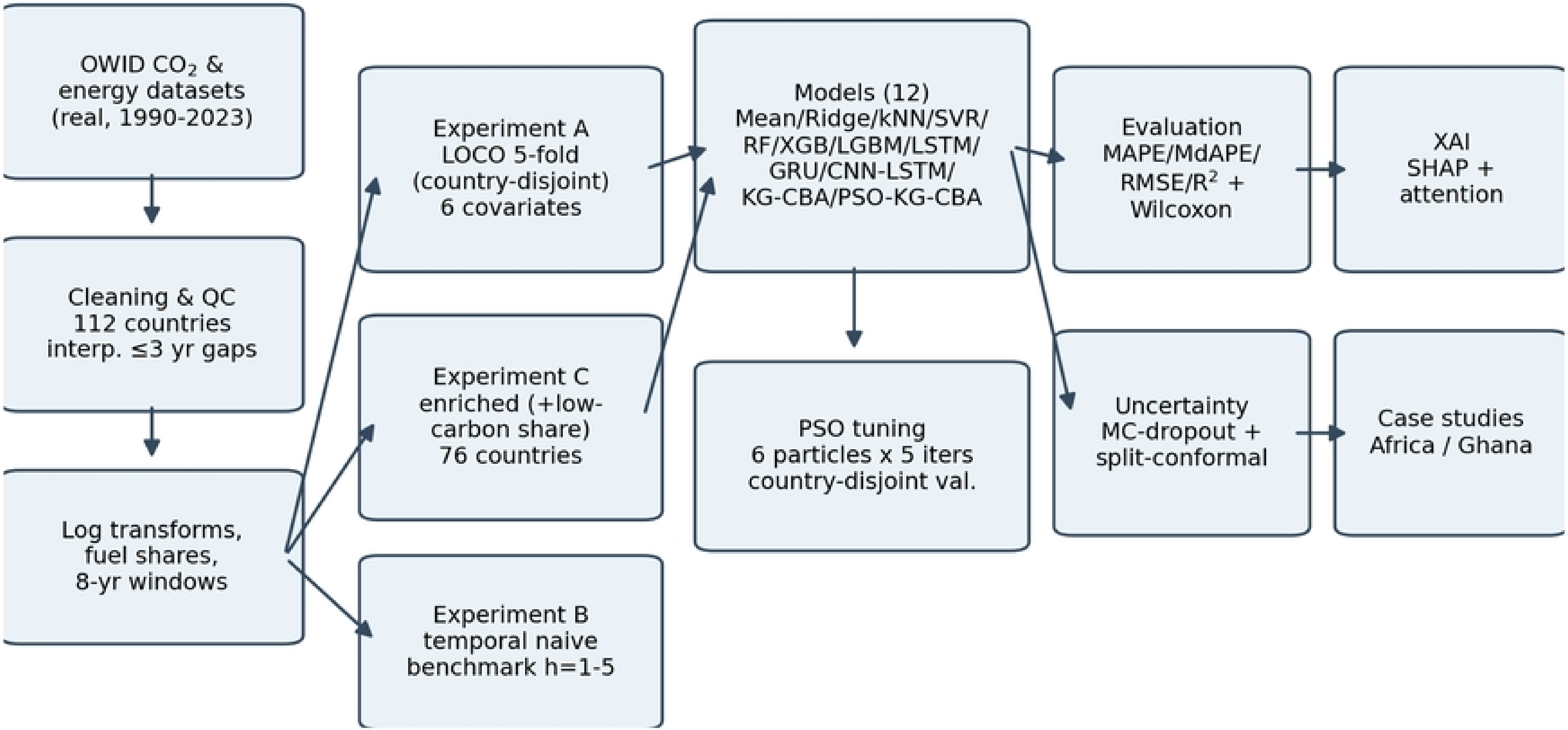

F04

Kaya-guided CNN-BiLSTM-Attention (KG-CBA): physics-informed linear backbone + deep residual branch

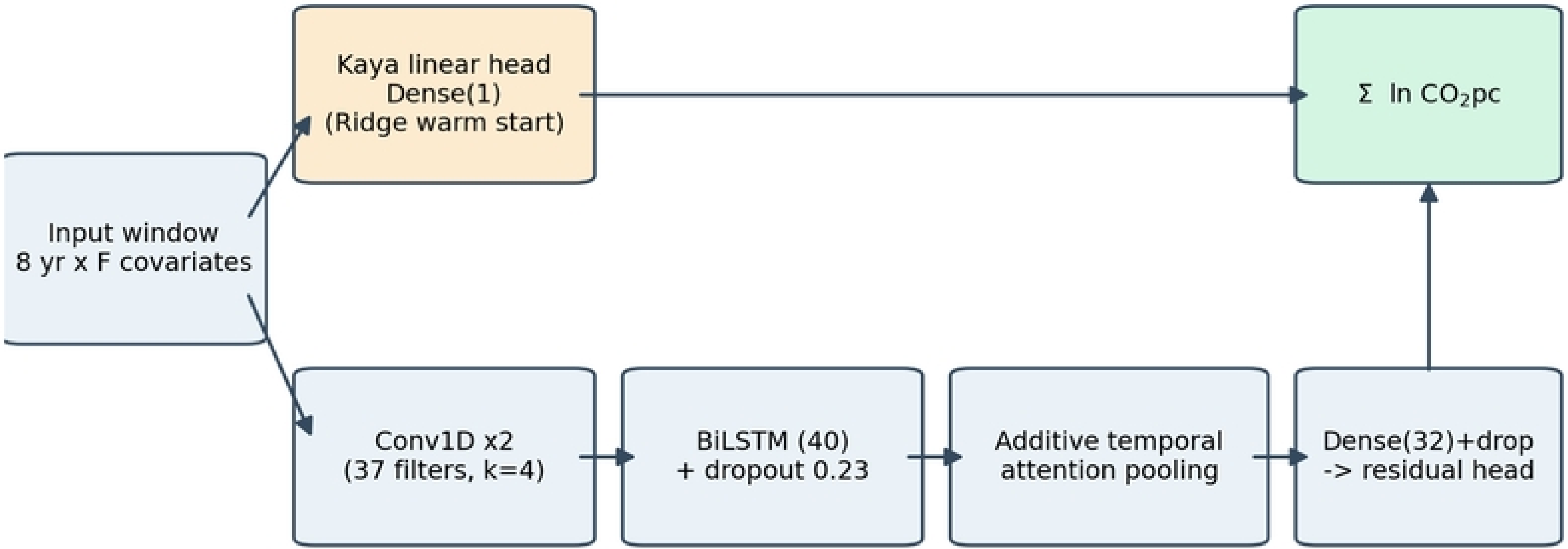

F05

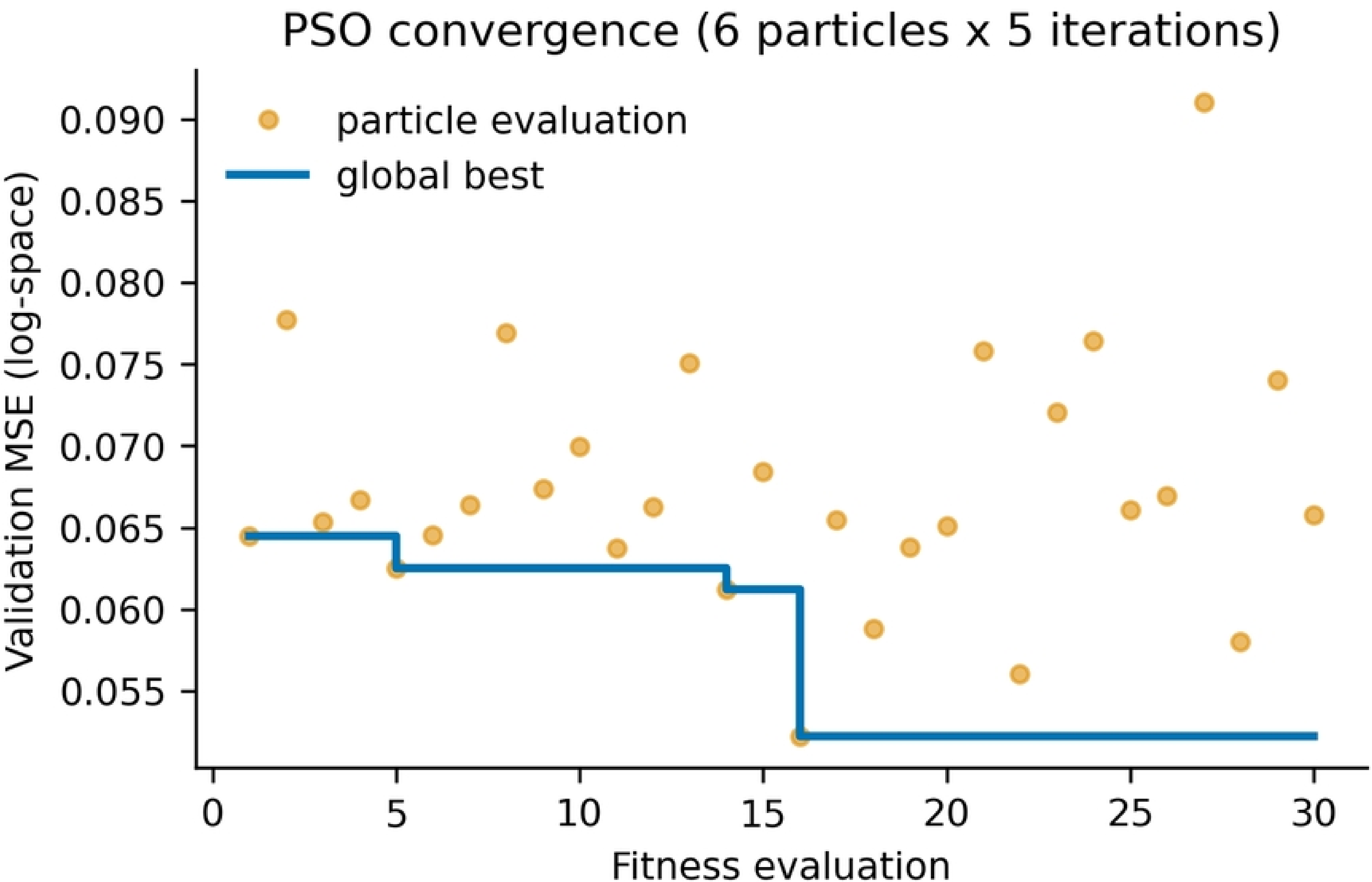
PSO convergence (6 particles x 5 iterations)
particle evaluation
global best
Validation MSE (log-space)
0.090
0.085
0.080
0.075
0.070
0.065
0.060
0.055
0
5
10
15
20
25
30
Fitness evaluation

F06

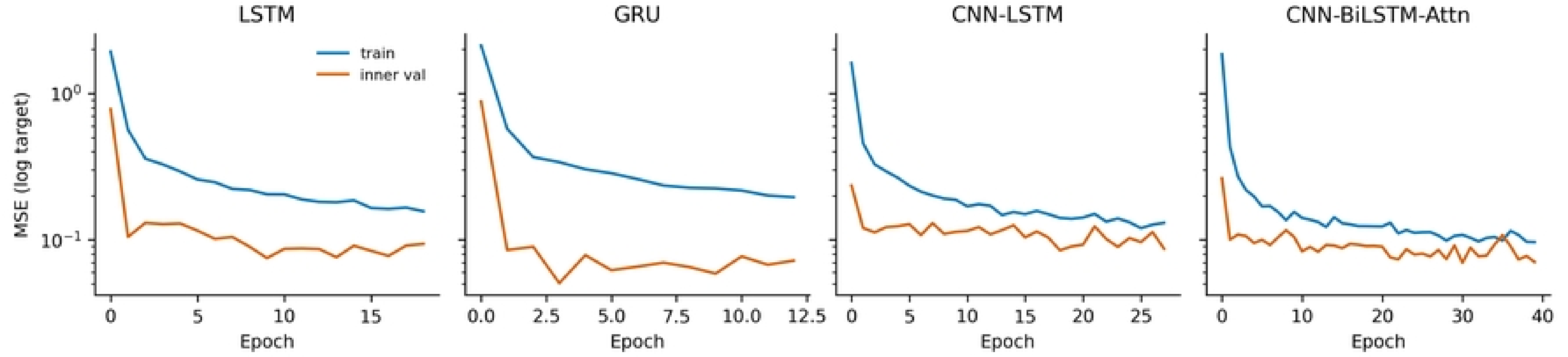
LSTM
GRU
CNN-LSTM
CNN-BiLSTM-Attn
train
inner val
MSE (log target)
10^0
10^{-1}
Epoch
0
5
10
15
0.0
2.5
5.0
7.5
10.0
12.5
20
25
30
40

F07

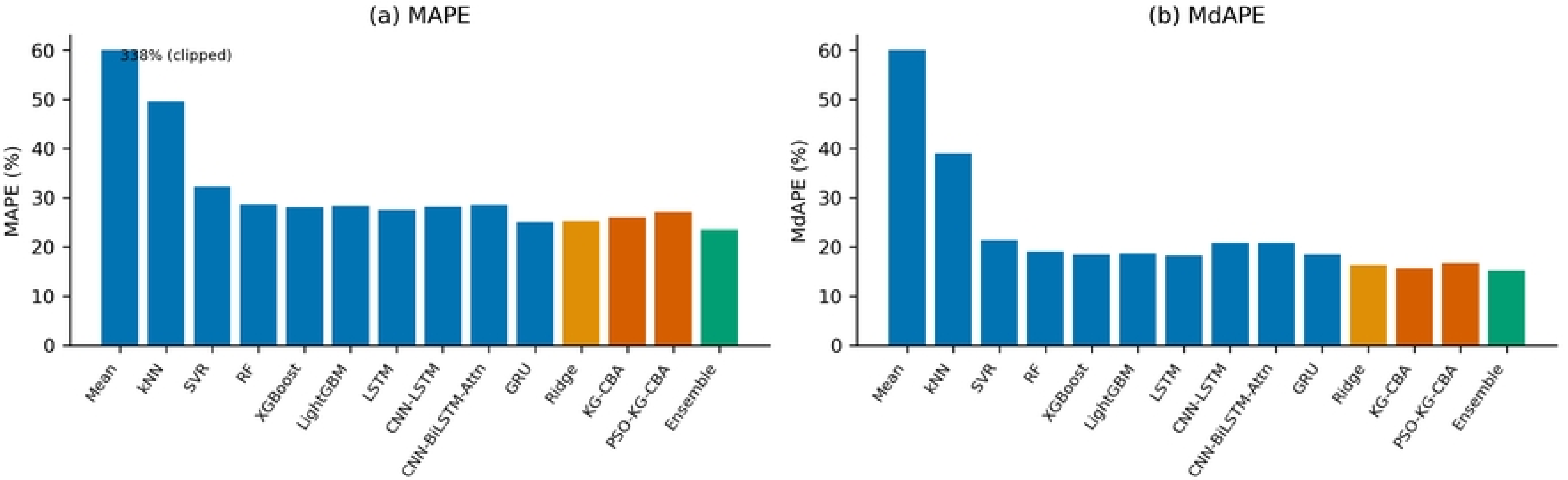

(a) MAPE
MAPE (%)
338% (clipped)
0
10
20
30
40
50
60
Mean
kNN
SVR
RF
XGBoost
LightGBM
LSTM
CNN-LSTM
CNN-BiLSTM-Attn
GRU
Ridge
KG-CBA
PSO-KG-CBA
Ensemble
(b) MdAPE
MdAPE (%)
0
10
20
30
40
50
60
Mean
kNN
SVR
RF
XGBoost
LightGBM
LSTM
CNN-LSTM
CNN-BiLSTM-Attn
GRU
Ridge
KG-CBA
PSO-KG-CBA
Ensemble

F08

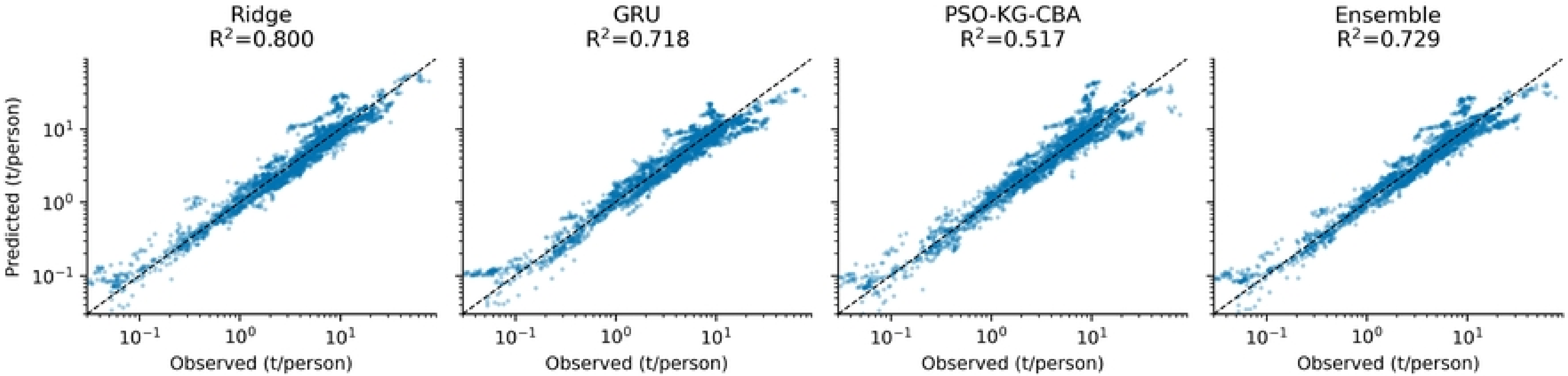

Ridge
R^2=0.800
GRU
R^2=0.718
PSO-KG-CBA
R^2=0.517
Ensemble
R^2=0.729
Predicted (t/person)
Observed (t/person)
10^{-1}
10^{0}
10^{1}

F09

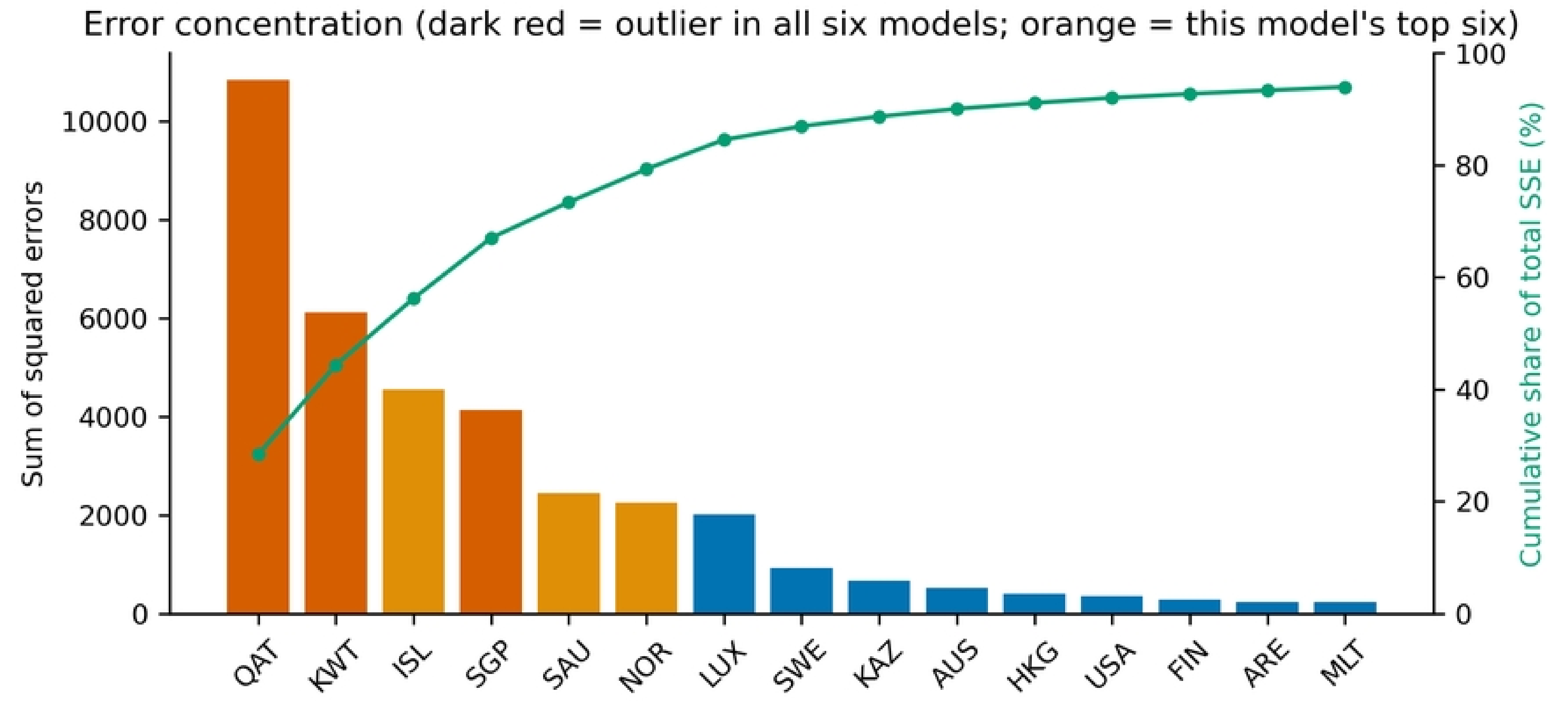

Error concentration (dark red = outlier in all six models; orange = this model's top six)
Sum of squared errors
Cumulative share of total SSE (%)
0
2000
4000
6000
8000
10000
0
20
40
60
80
100
QAT
KWT
ISL
SGP
SAU
NOR
LUX
SWE
KAZ
AUS
HKG
USA
FIN
ARE
MLT

F10

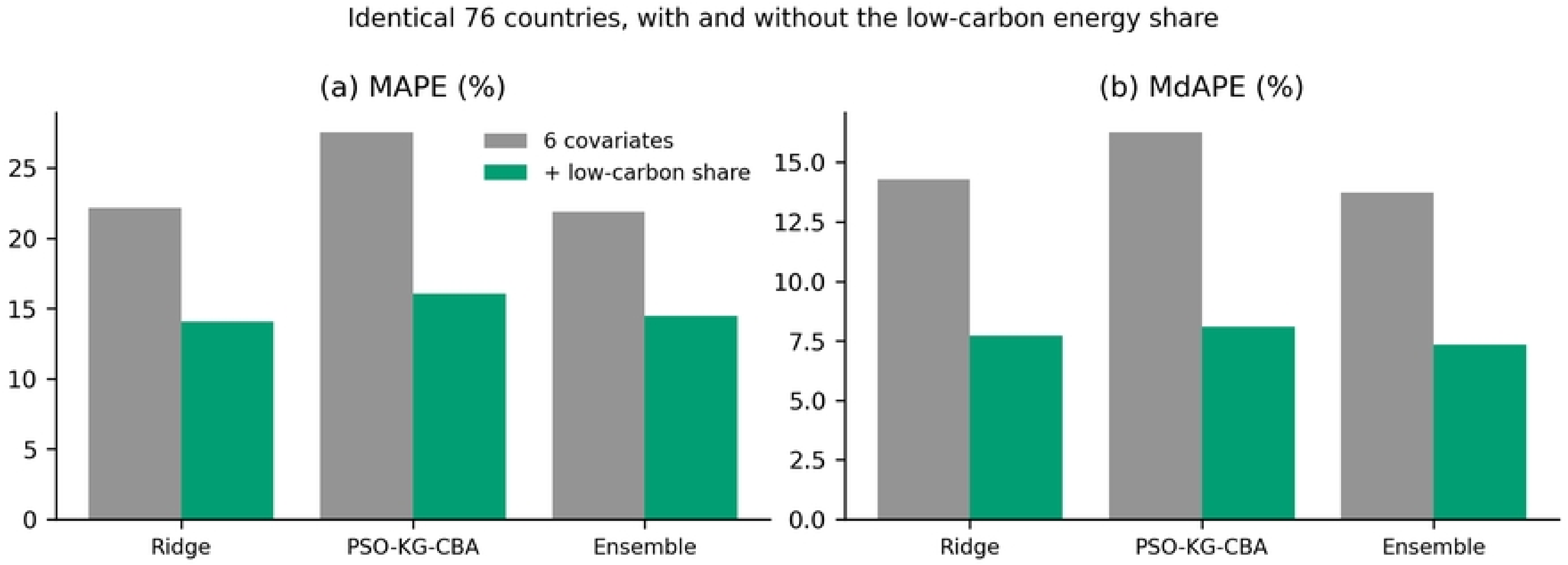
Identical 76 countries, with and without the low-carbon energy share
(a) MAPE (%)
(b) MdAPE (%)
6 covariates
+ low-carbon share
0
5
10
15
20
25
0.0
2.5
5.0
7.5
10.0
12.5
15.0
Ridge
PSO-KG-CBA
Ensemble

F11

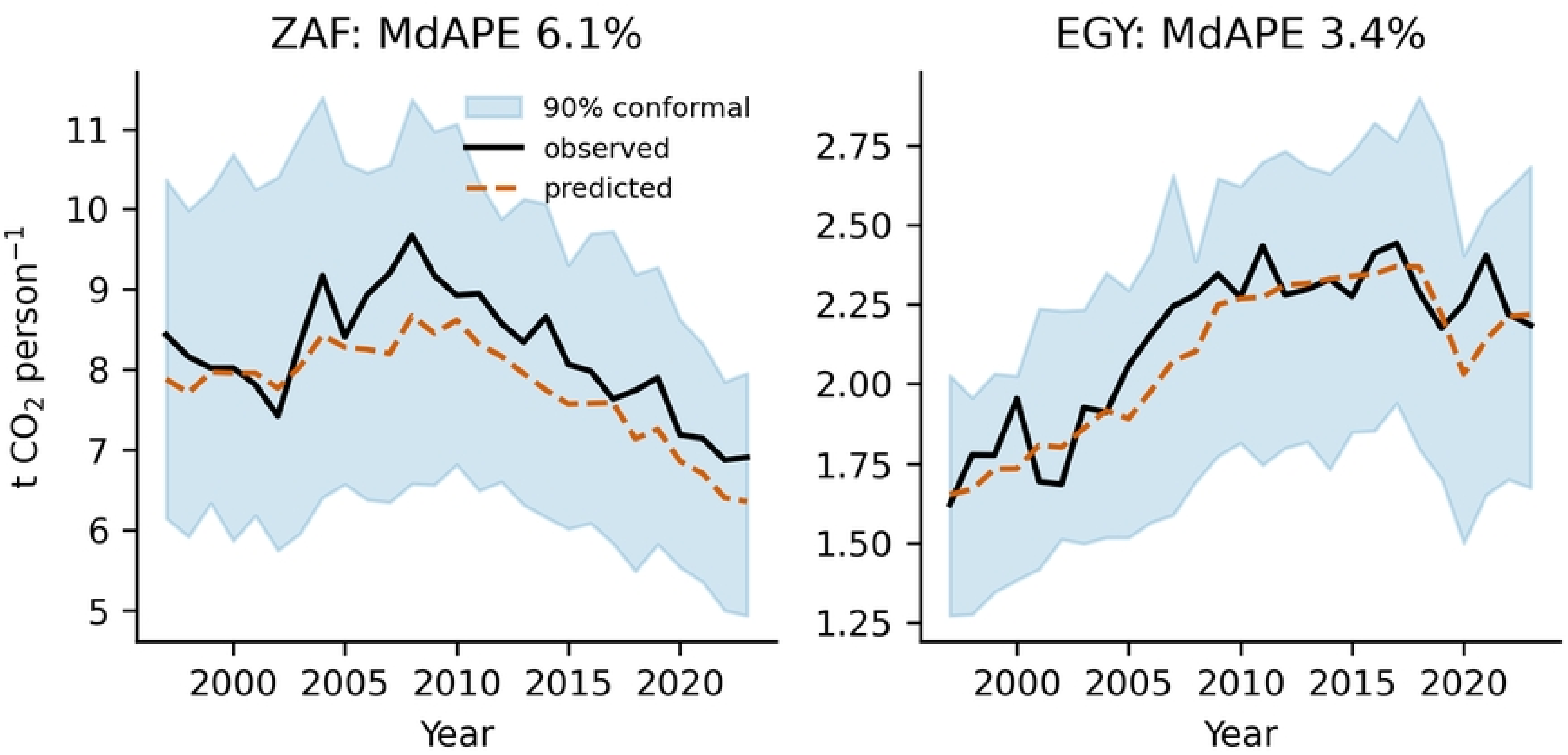

ZAF: MdAPE 6.1%
EGY: MdAPE 3.4%
90% conformal
observed
predicted
t CO_2 person^{-1}
Year
Year

F12

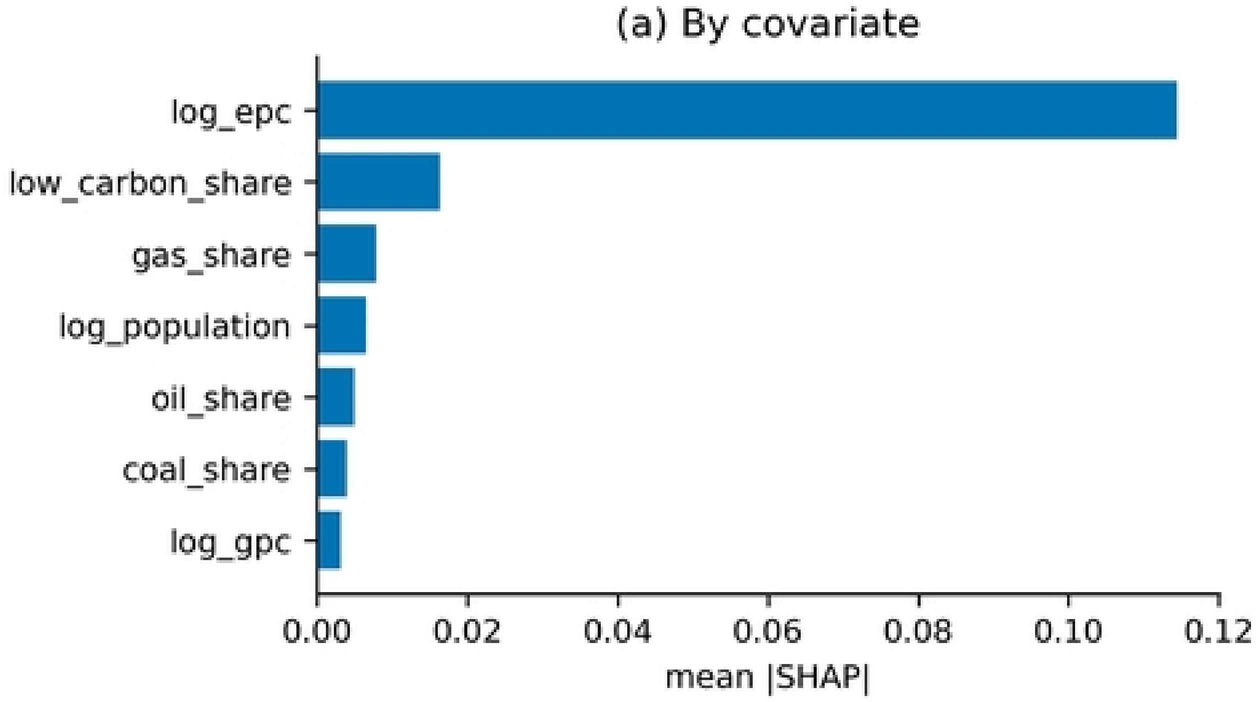
(a) By covariate
log_epc
low_carbon_share
gas_share
log_population
oil_share
coal_share
log_gpc
0.00
0.02
0.04
0.06
0.08
0.10
0.12
mean |SHAP|
(b) By window position
0.12
0.10
0.08
0.06
0.04
0.02
0.00
mean |SHAP|
t-7
t-6
t-5
t-4
t-3
t-2
t-1
t-0

F13

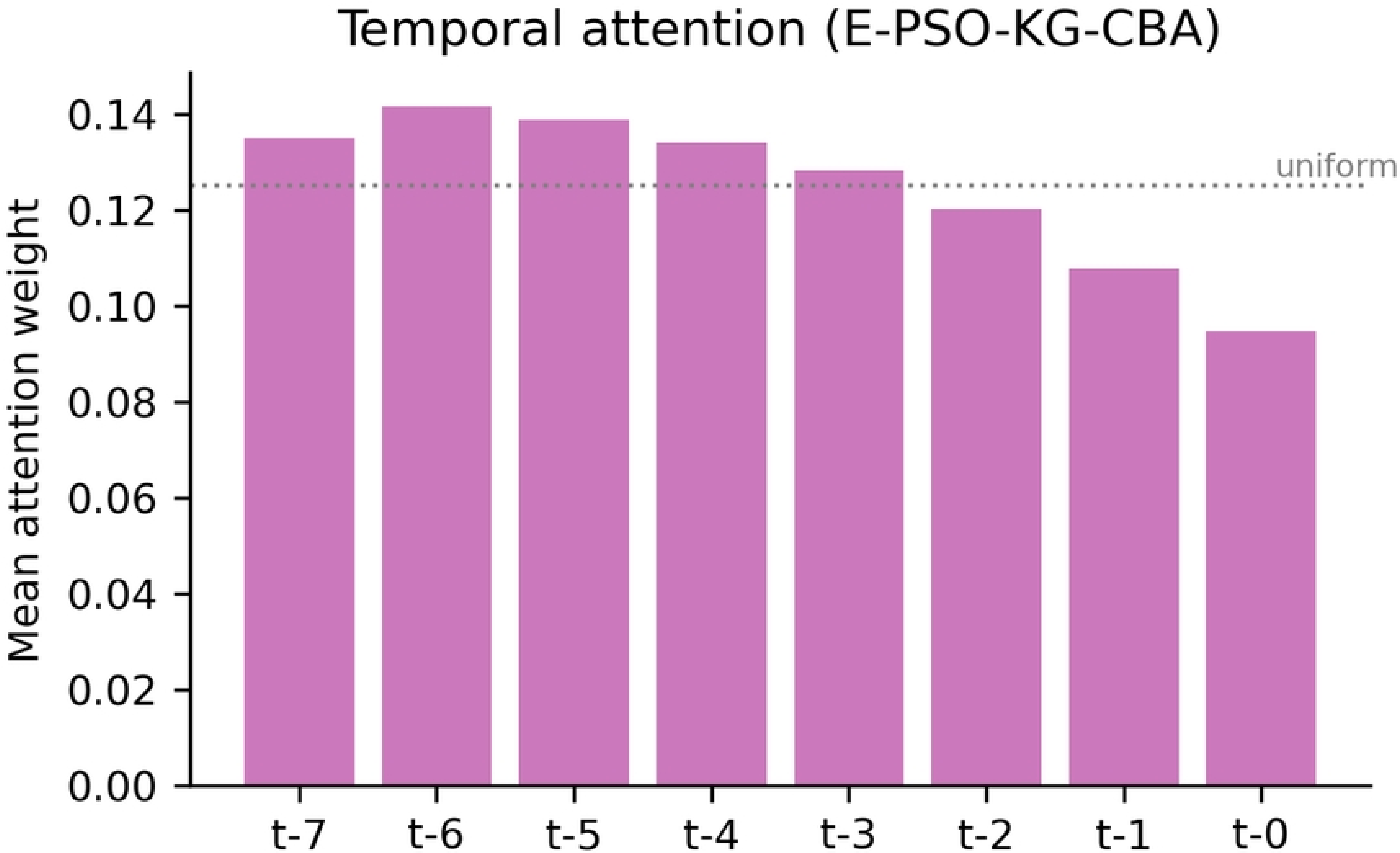
Temporal attention (E-PSO-KG-CBA)
Mean attention weight
0.00
0.02
0.04
0.06
0.08
0.10
0.12
0.14
uniform
t-7
t-6
t-5
t-4
t-3
t-2
t-1
t-0
F14

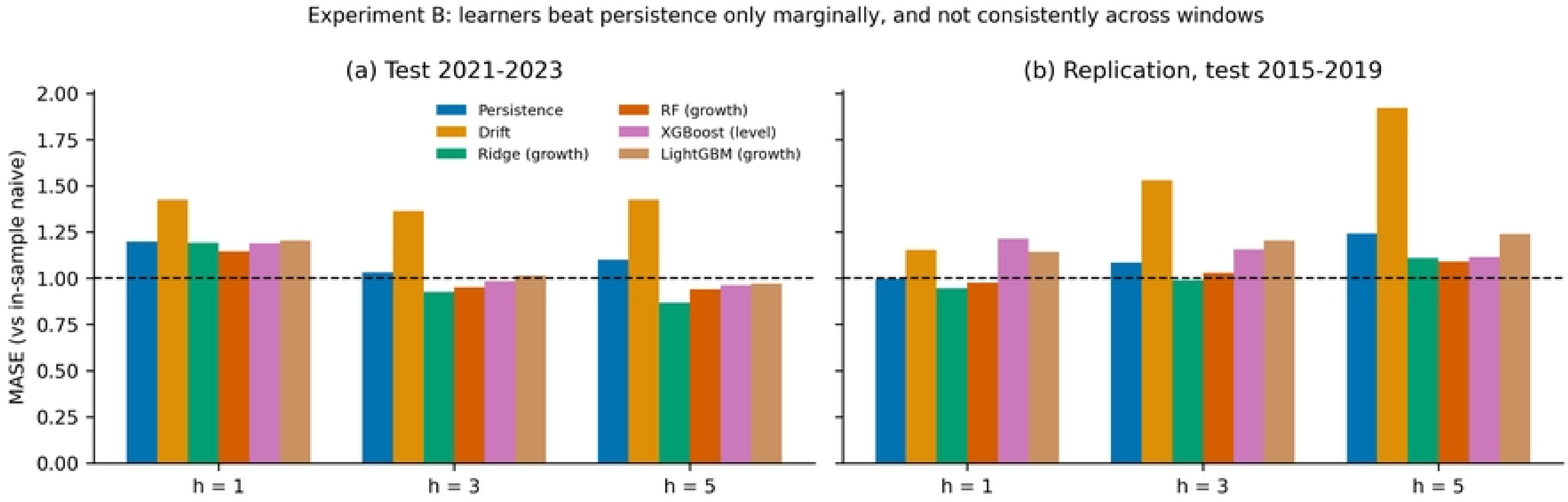
Experiment B: learners beat persistence only marginally, and not consistently across windows
(a) Test 2021-2023
(b) Replication, test 2015-2019
MASE (vs in-sample naive)
2.00
1.75
1.50
1.25
1.00
0.75
0.50
0.25
0.00
Persistence
Drift
Ridge (growth)
RF (growth)
XGBoost (level)
LightGBM (growth)
h = 1
h = 3
h = 5

F15